VŠB - TECHNICKÁ UNIVERZITA OSTRAVA

UNIVERZITNÍ STUDIJNÍ PROGRAMY

KATEDRA FYZIKY

NEUTRONOVÁ AKTIVAČNÍ ANALÝZA POMOCÍ GENERÁTORU 14 MeV NEUTRONŮ

NEUTRON ACTIVATION ANALYSIS USING 14 MeV NEUTRON GENERATOR

Autor: **Ing. Ondřej Harkut**

Vedoucí práce: **Doc. Dr. RNDr. Petr Alexa**

Ostrava 2017

VŠB - Technická univerzita Ostrava
Univerzitní studijní programy
Katedra fyziky

Zadání diplomové práce

Student: **Ing. Ondřej Harkut**

Studijní program: N1701 Fyzika

Studijní obor: 1702T001 Aplikovaná fyzika

Téma: Neutronová aktivační analýza pomocí generátoru 14 MeV neutronů
Neutron activation analysis using 14 MeV neutron generator

Jazyk vypracování: čeština

Zásady pro vypracování:

1. Rešerše literatury
2. Kalibrace neutronového generátoru
3. konstrukce potrubní pošty pro transport vzorků
4. Standardy pro neutronovou aktivační analýzu
5. Neutronová aktivační analýza krátkožijících izotopů

Seznam doporučené odborné literatury:

G. L. Molnár: Handbook of prompt gamma activation analysis with neutron beams, Kluwer Academic Press.

Formální náležitosti a rozsah diplomové práce stanoví pokyny pro vypracování zveřejněné na webových stránkách fakulty.

Vedoucí diplomové práce: **Doc. Dr.RNDr. Petr Alexa**

Datum zadání: 20.10.2016

Datum odevzdání: 15.05.2017

prof. Dr. RNDr. Jiří Luňáček
vedoucí katedry

prof. Ing. Petr Noskievič, CSc.
prorektor pro studium

VYSOKÁ ŠKOLA BÁŇSKÁ - TECHNICKÁ UNIVERZITA OSTRAVA
UNIVERZITNÍ STUDIJNÍ PROGRAMY

Čestné prohlášení

Prohlašuji, že předložená práce je mým původním autorským dílem, které jsem vypracoval samostatně. Veškerou literaturu a další zdroje, z nichž jsem při zpracování čerpal, v práci řádně cituji a jsou uvedeny v seznamu použité literatury.

V Ostravě dne 10. 5. 2017 Podpis 

Abstract

The purpose of this thesis is to examine the neutron flux of Thermo Fisher Scientific MP 320 14 MeV Neutron generator, construct pneumatic transport system for samples in the Laboratory for Neutron Activation Analysis and Gamma Spectrometry in Ostrava and present first detection of short-lived radionuclides using 14 MeV neutrons. The determination of neutron flux was performed by Texas convention technique. Successfully constructed pneumatic transport system was used during neutron activation of samples in which short-lived radionuclides were formed, to obtain gamma spectra of activated samples using scintillation spectrometer. Masses of selected isotopes in sample contents were analyzed by means of the results from neutron flux measurement and gamma spectrometry data of activated samples.

Keywords

Fast neutrons, Neutron Generator, Neutron Activation Analysis, Gamma Spectrometry

Abstrakt

Hlavním cílem práce je vyšetřit neutronový tok neutronového generátoru MP 320 od firmy Thermo Fisher Scientific, zkonstruovat transportní systém pro přenos vzorků v laboratoři pro neutronovou aktivační analýzu a gama spektrometrii v Ostravě a provést první testy detekce krátcežijících radionuklidů pomocí 14 MeV neutronů. Určení neutronového toku bylo provedeno pomocí metody Texaské konvence. Úspěšně zkonstruovaný pneumatický transportní systém byl použit během neutornové aktivace vzorků, v kterých byly aktivovány krátcežijící radionuklidy a přeneseny za pomocí transportního systému do scintilačního detektoru. Hmotnosti vybraných izotopů byly analyzovány z výsledků z měření neutronového toku a z dat získaných detektorem.

Klíčová slova

Rychlé neutrony, neutronový generátor, neutronová aktivační analýza, gama spektrometrie

Contents

List of Abbreviations

DGNAA ..... Delayed Gamma Neutron Activation Analysis

FNAA ..... Fast Neutron Activation Analysis

GS ..... Gamma Spectrometry

HPGe ..... High Purity Germanium

MCA ..... Multichannel Analyzer

NAA ..... Neutron Activation Analysis

NG ..... Neutron Generator

PGNAA ..... Prompt Gamma Neutron Activation Analysis

Introduction

Concern about D-T neutron generators as sources of 14 MeV neutrons has become significant due to their usage in neutron activation analysis, a nuclear method used for determination of elemental composition of various samples, and other applications of neutrons, such as neutron dosimetry calibration or neutron radiography. Neutron generators being sources of almost monoenergetic neutrons have been commercially provided by a number of manufacturers. In our case Thermo Fisher Scientific MP 320 Neutron Generator (NG) has been used.

Although D-T fusion provides monoenergetic neutrons, the resulting neutron flux of D-T generator shows slight deviations due to the changes with regard to an angle at which the neutron escapes the reaction. These effects need to be taken into consideration in determining the precise value of the neutron flux which is requested for neutron activation analysis calculations.

The determination of the neutron flux of MP 320 NG has been described and examined in this work. In order to carry out neutron activation analysis measurements this study has further investigated the efficiency of a scintillation spectrometer which has been used to collect gamma spectrometry data from samples activated by 14 MeV neutrons. The work also includes the description of pneumatic transport system constructed for transportation of samples containing short-lived radionuclides formed during 14 MeV activation. In the final part of the work selected short-lived radionuclides have been detected and their mass has been measured based on the results from neutron activation.

Chapters 1, 2 and 3 outline respectively the basics of radioactivity and gamma spectrometry, basic neutron properties and neutron activation analysis. Chapter 4 provides the calibration of NaI(Tl) scintillation spectrometer, chapter 5 refers about determination of the neutron flux of MP 320 NG and chapter 6 deals with measurements of short-lived radionuclides. Chapters 4, 5 and 6 are the major part of this work conducted by the author.

Chapter 1

Radioactive Decay and Gamma Spectrometry

Atomic nuclei can undergo a variety of processes that result in the emission of certain types of radiation. Such processes are **radioactive decay** and the interaction of a nucleus with another particle leading into **nuclear reaction**. Both processes are used in many applications from different fields of interest. This work mostly focuses on applications in elemental analysis of samples.

1.1 Law of Radioactive Decay

Radioactive decay is a random event producing ionizing radiation through nuclear rearrangement. If N is the number of radioactive nuclei contained in a sample at time t and -dN is the rate at which nuclei will decay in time dt, then the following relation [1] is valid

$$-dN = \lambda N dt, \tag{1.1}$$

in which the constant of proportionality λ is called the **disintegration constant** or the **decay constant**. $\lambda[s^{-1}]$ is a characteristic value for every radionuclide [2]. The integral solution of Eq. 1.1 [1], is the following

$$N = N_0 e^{-\lambda t} \tag{1.2}$$

where N_0 is the number of radioactive nuclei at time t=0 and N the number of radioactive nuclei at time t (remaining radioactive nuclei by that time). The radioactive decay process decreases exponentially over time. An important parameter related to the decay constant λ expressed by the following relation [3]

$$T_{1/2} = \frac{ln\ 2}{\lambda} \tag{1.3}$$

$T_{1/2}$ is called the **half-life** that measures how quickly radioactive nuclei decay. In one half-life, half of the number of original radioactive nuclei decay. Then, half of the remaining radioactive nuclei will decay in the next half-life and so on. The half-life is a character-

istic parameter for every radionuclide. It can vary from very short times (microseconds, seconds) to very long times of the magnitude of billions of years. Table 1.1 gives information on half-lifes of some selected radionuclides (data taken from Karlsruhe nuclide chart [4]).

Radionuclide	Half-life $T_{1/2}$
^{3}H	12.32 y
^{7}Be	53.28 d
^{14}C	5 715 y
^{18}F	110 min
^{22}Na	2.605 y
^{33}P	14.28 d
^{40}K	1.251×10^{9} y
^{53}Mn	3.7×10^{6} y
^{81}Kr	2.2×10^{5} y

Table 1.1: Half-lifes ($T_{1/2}$) of some radionuclides.

Usually the decay rate $A(= -dN/dt)$ [5] is more interesting than N for practical reasons. A more practical relation is obtained when rewriting Eq. 1.1 in terms of the decay rate A,

$$A = \lambda N. \tag{1.4}$$

In **Becquerel (Bq)** units, A is called the **activity** of a sample, defined as one decay per second

$$1 \text{ Bq} = 1 \text{ decay/s}.$$

When applying the activity A, an alternative law of radioactive decay [2] (Eq. 1.1) is used

$$A = A_0 e^{-\lambda t} \tag{1.5}$$

allowing to calculate the remaining activity A of a sample with initial activity A_0 for a time interval (t_0,t).

Radioactive decay can be carried out by three types of nuclear rearrangements leading to the emission of certain particles (radiation). Depending on what kind of particle is emitted, α, β or γ decays are observed. The following factors need to be taken into account: the conservations of electric charge, the number of nucleons, the momentum and the energy during radioactive decays. [6]

The radiation emitted in radioactive decay or in nuclear reactions (see Section 2.3) may be electromagnetic (e.g. γ-rays, x-rays) or corpuscular (e.g. α, β particles, neutrons and some others). Characteristics of some nuclear radiations are summarized in Table 1.2 (data from William [7]).

Type	Process	Charge	Mass of particle (MeV)
α particle	Nuclear decay or reaction	+2	3727.33
β^- particle	Nuclear decay	-1	0.511
β^+ particle	Nuclear decay	+1	0.511
γ photon	Nuclear de-excitation	0	0
X-ray	Atomic de-excitation	0	0
Neutron	Nuclear reaction	0	939.57

Table 1.2: Characteristics of some nuclear radiations.

The energy of an α particle decreases quickly due to its double charge, +2e. Uncharged radiation, such as neutrons, γ radiation and x-rays can penetrate matter more easily with less interaction. [7]

1.1.1 Alpha Decay

Radioactive decay α is a disintegration occurring in heavy nuclei of natural radionuclides with a characteristic half-life. While the nucleus is transformed into a different nuclide, a heavy α particle is emitted. The structure of the α particle was identified as a charged helium nucleus ${}^4_2\mathrm{He}^{2+}$. Due to the high binding energy of the helium nucleus, the particle does not disintegrate into individual nucleons (two protons, two neutrons) while leaving the nucleus. A parent nucleus X which undergoes alpha decay, rearranges according to the following equation [8]

$$ {}^A_Z\mathrm{X} \rightarrow {}^{A-4}_{Z-2}\mathrm{Y} + {}^4_2\mathrm{He}. \tag{1.6} $$

where A is the number of protons and neutrons (mass number) and Z is the proton number. During this decay, a daughter nucleus is created which often remains in an excited state and afterwards decays into its ground state releasing a gamma-ray. Alpha disintegration is the initial decay of the natural decay series found in nature. An example of alpha decay is shown below [5]

$$ {}^{238}\mathrm{U} \rightarrow {}^{234}\mathrm{Th} + {}^4\mathrm{He} $$

Uranium ${}^{238}U$ transforms via alpha decay into Thorium ^{234}Th. Table 1.3 (data from William [7]) shows characteristics of some alpha emitters.

Isotope	Half-life $T_{1/2}$	Energies (MeV)
^{241}Am	433 years	5.486, 5.443
^{210}Po	138 days	5.305
^{242}Cm	163 days	6.113, 6.070

Table 1.3: Characteristics of some aplha emitters.

1.1.2 Beta Decay

Radioactive decay of type β is a spontaneous process occurring in artificially produced radionuclides, lighter natural radionuclides and in actinides (radioactive natural chains). The process is often related to the changes inside the nucleus governed by the so-called

weak nuclear forces that is related to the subnuclear structure. If the nucleus undergoes beta decay, the mass number remains unchanged. Both charge and mass number are conserved. Beta decay is followed by emission of an **electron** ${}^{0}_{-1}e$ (β^- decay) or a **positron** ${}^{0}_{+1}e$ (positively charged particle with the same mass as an electron) as β^+ decay. A special case of β^+ decay called **electron capture** also occurs [3]

- β^- **decay** follows the decay mode

$$ {}^{A}_{Z}\mathrm{X} \rightarrow {}^{A}_{Z+1}\mathrm{Y} + {}^{0}_{-1}e + \bar{\nu}_e \tag{1.7} $$

  where $\bar{\nu}$ represents a particle called antineutrino. The daughter nucleus Y contains an extra proton because a neutron transforms into a proton and at the same time an electron and an antineutrino are emitted. An example of β^- decay mode within a nucleus is shown below

$$ {}^{32}\mathrm{P} \rightarrow {}^{32}\mathrm{S} + e^- + \bar{\nu}_e. $$

- β^+ **decay** - a parent nucleus undergoing β^+ decay changes its nuclear arrangement according to this relation

$$ {}^{A}_{Z}\mathrm{X} \rightarrow {}^{A}_{Z-1}\mathrm{Y} + {}^{0}_{1}e + \nu_e \tag{1.8} $$

  where ν is a particle called electron neutrino. The parent nucleus emits positively charged positron and neutrino. During the nuclear rearrangement a proton inside a nucleus transforms into a neutron leading to the production of a positron and a neutrino. Following example represents β^+ radioactive decay

$$ {}^{64}\mathrm{Cu} \rightarrow {}^{64}\mathrm{Ni} + e^+ + \nu_e \tag{1.9} $$

  If a positron source is enclosed in an absorbing material, the positrons will annihilate the electrons in the absorber and this process will produce two photons, each carrying an energy equal to the electron rest mass 511 keV and opposite direction of motion. [1]

- **Electron capture** - an electron located in an atomic shell is captured by a nucleus resulting in the transformation of a proton into a neutron. This process can be described by the following equation

$$ {}^{0}_{-1}\beta + {}^{A}_{Z}\mathrm{X} \rightarrow {}^{A}_{Z-1}\mathrm{Y} + \nu_e. \tag{1.10} $$

  Since an electron shell lacks an electron at its lowest energy level, it is filled with a nearby electron from higher energy level. This leads to the emission of x-ray radiation typical for each element, e.g.

$$ {}^{55}\mathrm{Fe} + e^- \rightarrow {}^{55}\mathrm{Mn} + \nu_e \tag{1.11} $$

$$ \mathrm{E}_{K_\alpha} = 5.9 \text{ keV} $$

$$ \mathrm{E}_{K_\beta} = 6.5 \text{ keV}, $$

  E stands for x-ray energies, α and β represent different kinds of transition energies. [7]

1.1.3 Gamma Emission

A nucleus that decays spontaneously by emitting an α or β particle usually ends up in an excited state with extra energy. When this energy is released, the nucleus decays into a more stable ground state and γ photon or many photons with a certain energy are emitted. Life-times of these excited-state nuclei are generally very short and the photon is basically radiated away at the same time as the α or β particle. γ radiation belongs to the electromagnetic radiation, the same as for example x-rays or light, but with much shorter wavelengths (in order of 10^{-13} m) [6]. Cesium ^{137}Cs is a radioisotope which decays by β^- decay to barium ^{137}Ba [7]

$$^{137}\mathrm{Cs} \rightarrow \ ^{137}\mathrm{Ba}^* + e^- + \bar{\nu} \tag{1.12}$$

where * denotes the excited state of barium ^{137}Ba. It de-excites to the ground state releasing a quantum of energy

$$^{137}\mathrm{Ba}^* \rightarrow \ ^{137}\mathrm{Ba} + \gamma \ (661.7 \ keV). \tag{1.13}$$

Gamma rays emitted during de-excitations of the nuclei play a significant role in a method named **gamma spectrometry** [2] (see Section 1.3).

1.2 Sources of Ionizing Radiation

Organisms of the planet Earth have adapted to the **natural radioactivity** originating from many sources that surround them. There are three distinct categories categorized based on the origin of production of the radionuclide

1. cosmogenic radionuclides
2. primordial radionuclides
3. radioactive decay series

The distribution of natural radioactive sources on Earth is constantly modified by human actions such as fertilizer production, fossil fuel use or anthropogenically produced radionuclides. So-called **artificial radioactivity** of human-produced radionuclides and radiation after the nuclear era has also a contribution to the radiation dose. Nowadays a part of radiation dose is caused by **medical radiation** coming from radiodiagnostic, radiotherapy or nuclear medicine techniques used in modern medicine. [8]

Both natural and artificial radioactivity create a radioactive background radiation that disrupts sensitive measurements of radioactive samples in radioanalytical methods, e.g. gamma spectrometry (Section 1.3). [2]

Natural Radioactivity

The planet Earth is permanently bombarded by incoming cosmic radiation of high-energy paricles origintaing in galactic cosmic radiation and solar cosmic radiation, so-called galactic and solar wind, respectively. Cosmic radiation composition varies greatly. Galactic cos-

mic radiation typically consists of protons (87%), α particles (11%), heavier nuclei ($\sim$ 1%) and high-energy electrons ($\sim$ 1%). Solar wind is composed principally of higher proton composition (98%) and α particle contribution is only about 2%. When entering the Earth's atmosphere, cosmic radiation interacts with the atmosphere's particles leading to nuclear reactions which produce cosmogenic radionuclides contributing to the total radiation dose of natural radioactivity. The main contribution belongs to the cosmogenic radioisotopes, such as ^{3}H, ^{7}Be, ^{14}C and ^{22}Na. [8]

Radioactivity from primordial radionuclides, defined as radionuclides present since the formation of the Earth which have half-lifes comparable to the age of the Earth ($T_{1/2} \sim 4.5 \cdot 10^{7}$ years), has about 16.5% contribution to the world average anual dose of natural radioactivity mainly emanating from potassium ^{40}K and rubidium ^{87}Rb. [8]

Special case of primordial radionuclides are those which create natural decay series. Natural radioactivity related to the dose resulting from such radionuclides has the vast majority that contributes to the anual radiation dose of natural sources of all three categories, over 80%. There are nowadays three natural decay series with original primordial radionuclides ^{232}Th, ^{238}U and ^{235}U. They all have some common characteristics

1. They originate from primordial radionuclides with half-life over 10^{8} years.
2. They possess a gaseous radioisotope of radon in the series.
3. They end with a stable isotope of lead.
4. They decay via a series of α and β transformations.

Some uncommon natural sources of radioactivity associated with uranium are found in uranium-containing materials or spontaneous fission in uranium ores so-called natural nuclear reactors. [8]

Artificial Radioactivity

Artifial radioactivity comes from the sources provided by human actions such as nuclear explosions, nuclear accidents, routine releases from nuclear reactors, nuclear medicine, releases due to nuclear weapon or nuclear fuel production etc. Some of such produced radioisotopes may be found in natural samples, for example ^{137}Cs from Chernobyl explosion is now still found in the environment. Also the materials from which radiation detectors are made can contain some impurities so only radiopure materials should be used. [8]

1.3 Gamma Spectrometry

Gamma spectrometry provides direct determination of individual radionuclides in gamma emitting samples by measuring these gamma pulses as counts arranged according to the energy. During the nuclear transitions in radioactive sample, the nuclei may undergo de-excitations by releasing gamma energies that are characteristics of specific radionuclides.

All the gamma rays emitted by the source are unique signatures of its isotopical composition. However some limitations of this method arise here. If the source contains only pure beta or alpha emitters, the composition cannot be determined by gamma spectrometry. But from what is known most of beta transitions go to an excited state first before going to the ground state of daughter nucleus. [9]

1.3.1 Nuclear Decay Scheme and Gamma Spectrum

In order to represent the transitions and changes inside a nucleus, they are diagrammed into the **decay scheme**. The decay scheme is usually plotted in the following way. It is represented in a coordinate system in which the vertical axis is energy, increasing from bottom to top and the horizontal axis is the number of protons, increasing from left to right. The arrows indicate the released particles. Half-lifes (year), emission probability of particles P_γ and energy E_γ (keV) are also given. Fig. 1.1 [2] represents the nuclear rearrangement within the nucleus of cesium ^{137}Cs and cobalt ^{60}Co. In the case of ^{137}Cs, 661.7 keV is the only gamma energy in the scheme. In the scheme of ^{60}Co more transitions are involved. Two gamma rays γ_1 and γ_2 appear during the nuclear transformtaion. Each of them carries an energy being the difference between the energies of the upper and lower level as following

$$\gamma_1 = 2505.7 - 1332.5 = 1173.2 \text{ keV}$$

$$\gamma_2 = 1332.5 - 0 = 1332.5 \text{ keV}.$$

In addition to γ_1 and γ_2 a coincidence may happen when the two gamma-ray energy are measured at essentially the same time and third gamma ray may be detected ($\gamma_3 = \gamma_1 + \gamma_2 = 2505.7$ keV).

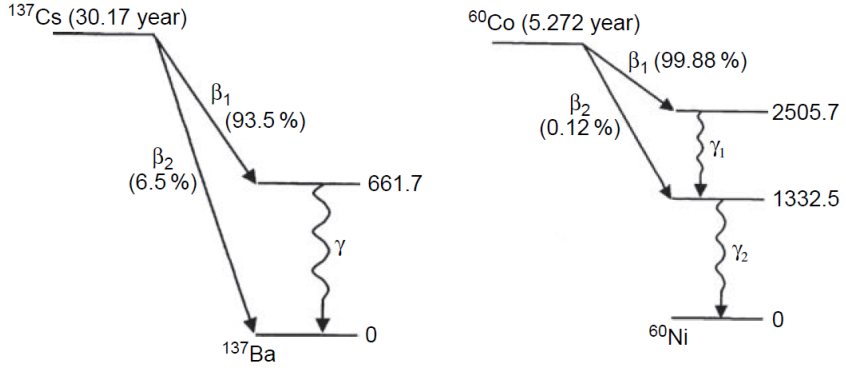

Figure 1.1: The decay schemes of ^{137}Cs (left) and ^{60}Co (right) [2].

If a gamma source is properly measured, its gamma-rays are detected and organized into a histogram, so-called **gamma spectrum** [2]. The horizontal axis divides the spectrum according to energy in keV or MeV and the vertical axis counts gamma pulses detected from the source. One can then read all gamma energies released from the sample and its analysis may be proceeded. Radiation from background surrounding the detector must be taken into account and substracted from the analysis and calculations. Fig. 1.2 illustrates natural

background in the Laboratory for Neutron Activation Analysis and Gamma spectrometry at VŠB-TU Ostrava (more detail in Chapter 6). It was measured for 113772 seconds on the germanium spectrometer (see Part 1.3.3).

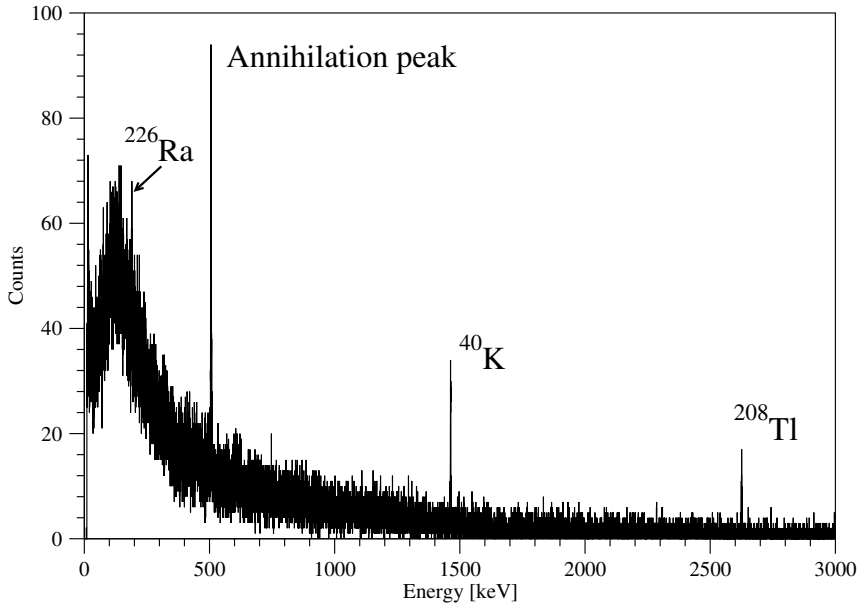

Figure 1.2: Gamma spectrum of background radiation measured in the Laboratory of Neutron Activation Analysis and Gamma Spectrometry at VŠB-TU Ostrava, Czech Republic.

There are three significant peaks and one minor peak in the background spectrum: annihilation peak, ^{40}K, ^{208}Tl and ^{226}Ra decay peaks. Annihilation peak at 511 keV observed in the spectrum originates from annihilation of positrons. Photopeak at 1461 keV confirms the presence of natural radionuclide ^{40}K which decays to ^{40}Ar through electron capture and the furthest photopeak at 2614.5 keV refers to the highest gamma energy naturally occuring in the environment released during β^- transformation of thalium to lead. Radium ^{226}Ra decays via α transformation into ^{222}Rn followed by the emission of gamma energy 186.2 keV (data taken from Gilmore [2], Appendix D: Gamma-Ray Energies in the Detector Background and the Environment and The Lund/LBNL Nuclear Data Search Database [10]).

1.3.2 Interactions of Photons with Matter

When γ ray encounters a matter, it can undergo several processes that lead to different types of interaction. Such interactions depend upon the energy of the radiation and material which the radiation interacts with [11]. In gamma spectrometry usually germanium or sodium iodide are used for detection material and lead as shielding material [2]. Attenuation coefficient is formulated as a function of gamma energy expressing how easily a certain material can be penetrated by gamma rays. In Fig. 1.3 the attenuation coefficient of germanium is displayed.

The total attenuation coefficient is the sum of curves due to the three interactions of γ pho-

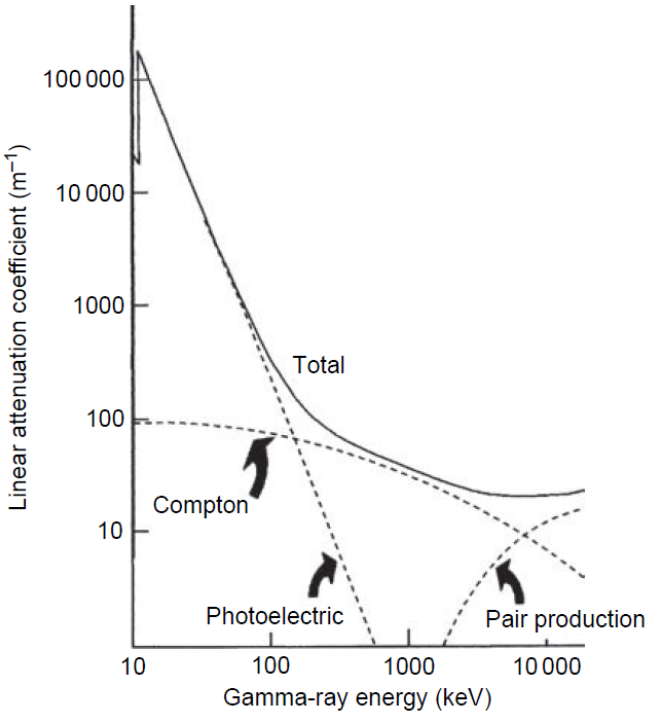

Figure 1.3: The attenuation coefficient of germaium as a function of gamma energy [2].

ton with germanium matter: **photoelectric effect**, **compton scattering** and **pair production**. If γ photon undergoes photoelectric effect, it ejects a bound electron from material's atom and is fully absorbed by the electron. The empty shell is then filled with the closest electron which leads to the emission of characteristic x-ray. Compton scattering is an interaction of photon with electron as well but only a part of the energy is transferred to the interacting electron which then recoils and the photon is scattered with less energy. Such scattered photon can further undergo some interaction. Pair production on the other hand is interaction of photon with the atom as a whole. The process takes place in Coloumb field of the nucleus where high energy photon converts into an electron-positron pair. Positrons will almost immediately annihilate with surrounding electrons resulting into two annihilation photons, each carrying energy of 511 keV. The annihilation photon can further interact with the material in one of the three processes. [2]

Photoelectric effect is dominant at low energy, compton scattering in the mid-energy range and pair production appears only at an energy higher than 1.022 MeV. **Cross section** σ of each interaction expresses the probability that a photon will undergo photoelectric absorption, compton scattering and pair production, respectively. The total cross section for all types of interaction is the sum of all three

$$\sigma_{tot} = \sigma_{PE} + \sigma_{CS} + \sigma_{PP}. \tag{1.14}$$

The attenuation coefficient is directly proportional to the corresponding cross section. A gamma-ray of a specific energy can undergo either photoelectric effect, compton scattering or pair production if the energy is high enough. This results to additional possibilities for interaction within the detector. [2]

In Fig. 1.4 there is an illustration of detector and three primary gamma rays γ_1, γ_2 and γ_3. γ_1 interacts with the detector by photoelectric effect (PE) and the whole gamma ray energy is transfered to electrons in the detector. After this no additional gamma energy is available and current created by γ_1 can be collected. γ_2 undergoes compton scattering (CS) followed by second compton scattering which creates lower energy photon which can either escape the detector or scatter again. γ_3 transforms into positron and electron which then annihilate and create additional photons γ_{511} that may interact as photoelectric effect, compton scattering or escape the detector.. All the events within the detector creates an electric current that is collected and processed into gamma spectrum. Photopeak carries the significant information about the radionuclide that is measured. Other attributes in the spectrum resulting from additional events of compton scattering and pair production may unintentionally ruin important information about the measured radioactive sample. [2]

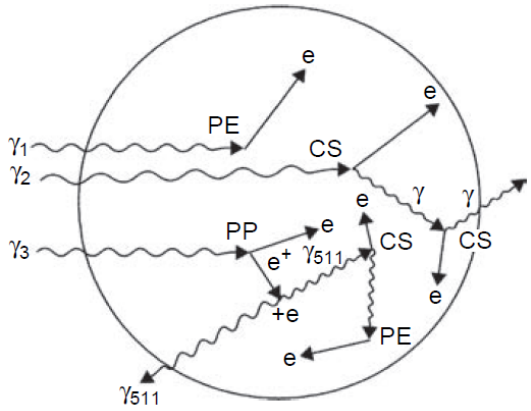

Figure 1.4: Additional events within a detector [2].

Following Fig. 1.5 is a gamma spectrum of ^{137}Cs decaying through beta transformation followed by gamma emission of energy 661.7 keV. Full energy peak of 661.7 keV can be clearly seen in the spectrum accompanied with other features resulting from the interactions mentioned above.

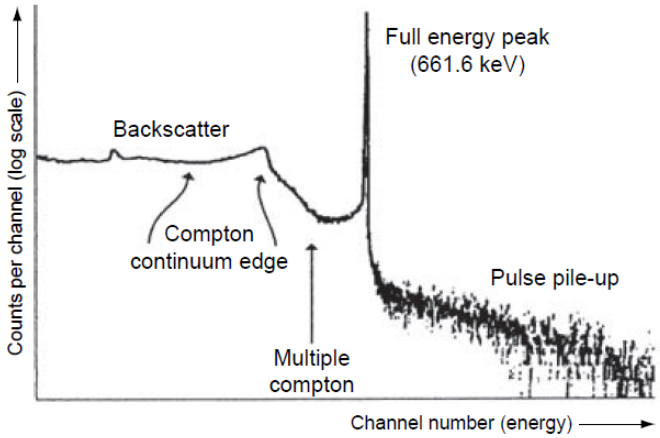

Figure 1.5: Example spectrum illustrating the various spectral features of ^{137}Cs [2].

Backscatter is a low and wide peak within the broad range 200-300 keV resulting from gamma-rays scattered through a large angle by the shielding. Compton continuum edge and multiple compton are results from the multiple compton scattering within the detector during which photons from the source are differently scattered carrying various energies creating this continuum in the spectrum. Pulse pile-up continuum refers to random summing, two gamma-rays being detected at the same time and therefore located behind the full energy peak. [2]

1.3.3 Gamma Spectrometer

Two of the most often and widely used detectors in gamma spectrometry are scintillation detectors and semiconductor detectors. In gamma spectrometry these are called **gamma spectrometers** for their properties to be able to measure the amount of ionization gamma energy deposited in the detection crystal. To measure multiple energies released from a gamma source **MCA** (multichannel analyzer) is to be used. [7]

Gamma spectrometry using scintillation spectrometer (schematic Fig. 1.6) makes a use of the fact that certain materials emit a small flash of light while being strucked by a gamma-rays. As far as the scintillation detectors are concerned, many different types of material with scintillation ability may be used. In gamma spectrometry the most commonly used material is a crystal NaI(Tl), Natrium Iodide activated by Thalium. The crystal is placed close to a photomultiplier, amplifying device, that amplifies the flashes of light by cascade of dynodes and converts them into electrical pulses which are further processed into a gamma spectrum carrying information concerning the incident gamma radiation. Scintillators request not to be cooled down like semiconductor spectrometers. On the other hand the energy resolution of scintillation detectors is much worse than at semiconductor detectors. This results to a problem with distinguishing close-lying energies in a spectrum. [7]

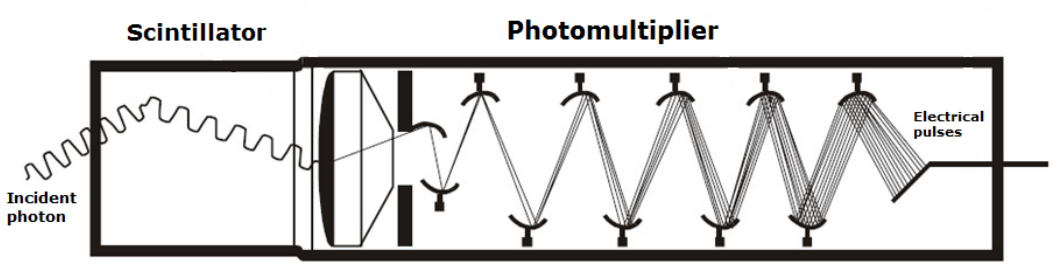

Figure 1.6: Schematic diagram of a scintillation spectrometer.

Semiconductor spectrometer used in gamma spectrometry is most often consisted of high purity Germanium crystal (HPGe). The ionization energy passing through the crystal creates electron-hole pairs (charge carriers) which are then collected by an electric field forming information about the incident energy. Germanium spectrometers require cooling system added to spectrometer setup. Before the semiconductor crystal can operate,

low temperatures must be achieved. Unlike scintillators, semiconductors have far greater energy resolution which allows to separate very close peaks in a spectrum. [2]

In order to know the exact gamma energies contained in a sample and to calculate the activity produced by the sample, energy and efficiency calibrations need to be performed.

Energy calibration expresses the relationship between channels and energy. Each channel in MCA must be assigned to energy E so the right position of the peak is known. Energy calibration is accomplised by measuring a spectrum of radionuclide with precisely known energies, then the real energies of the radionuclide can be assigned to the measured peak positions. Source used for energy calibration can be consisted of either a single nuclide with more gamma energies or several nuclides, for example ^{152}Eu as a single nuclide covering wide range of energies. However, some nuclides allow only a two point linear calibration (e.g. ^{60}Co releases two gamma energies) [2]

$$E(\text{keV}) = I(\text{keV}) + G \cdot Ch(\text{Channels}) \tag{1.15}$$

By measuring the spectrum of ^{60}Co this linear approximation is calculated and energies can be assigned to channels. Two parameters I and G must be determined from the linear approximation.

Efficiency calibration is based on the fact that each gamma energy is detected with different efficiency by a spectrometer crystal. Lower energies may be detected better than high energetic gamma-rays that escape the crystal more easily undetected. Efficiency calibration expresses the relationship between the number of counts and disintegration rate. It is performed on actual gamma-ray spectra. By measuring wide range energy spectra it is possible to construct an efficiency curve as a plot of efficiency against energy. While energy of the gamma source is known, efficiency ε calculation follows this relationship [2]

$$\varepsilon = \frac{R}{A \cdot P_\gamma} \tag{1.16}$$

where $R = (C/t)$ is the number of counts of the peak (peak area) C over the measured time in seconds t, A is the activity of the source and P_γ is the probability of emission of the particular gamma-ray.

Using the efficiency calibration the spectrometer response to different gamma energies is well known. Hence unknown samples may be measured and their spectra processed with respect to gamma sources contained in the samples. To determine the activity of the sample from gamma spectrometry data, following equation is used [2]

$$A = \frac{R}{\varepsilon \cdot P_\gamma}. \tag{1.17}$$

Chapter 2

Neutrons

The neutron was discovered by **James Chadwick** (∗1891 - † 1974) [12] while he undertook a serie of experiments searching for neutron. In 1932 Chadwick finally achieved his goal and confirmed the existence of unknown particle until that time. Chadwick recognized some serious difficulties in conclusions of Boethe and Becker and Irene and Frederic Joliot-Curie from the experiment producing penetrating radiation produced by bombardment of beryllium by α particles. Chadwick observed the number of protons in the nuclear reaction was not conserved and the calculated energy was less than the measured energy. Chadwick carried out several experiment setup during which he irradiated different materials, containing helium, lithium, beryllium, boron, argon, carbon, oxygen and nitrogen. He combined all the experiment measurements and came to a conclusion that the unknown radiation consisted of uncharged particles of mass

$$m_n = 1.15 \text{ u},$$

where u represents atomic mass unit [3]

$$1 \text{ u} = 1.660\ 538\ 86 \times 10^{-27}\text{kg}. \tag{2.1}$$

The transformation of beryllium nucleus caused by the bombardment of α particles leads to a production of neutrons with the similar mass as protons in a reaction (n,α) represented by

$${}^4_2\text{He} + {}^9_4\text{Be} \rightarrow {}^{12}_6\text{C} + {}^1_0 n \tag{2.2}$$

Later a second more precise measurement was performed by Chadwick and better estimate of neutron mass was achieved by replacing the beryllium nucleus with a boron nucleus forming the reaction

$${}^4_2\text{He} + {}^{11}_5\text{B} \rightarrow {}^{14}_7\text{N} + {}^1_0 n \tag{2.3}$$

In order to calculate mass of neutron from the nuclear reaction (2.3) the masses of ${}^4_2$He, ${}^{11}_5$B and ${}^{14}_7$N and kinetic energies T of initial and final particles must be known. The masses were obtained from mass spectroscopy and the energies were measured or calculated from conservation of momentum. Applying the Einstein relation for rest mass energy $E = mc^2$

to in Eq. 2.3, the coservation of energy must hold

$$(m_\alpha + m_B)c^2 + T_\alpha \rightarrow \ (m_N + m_n)c^2 + T_N + T_n. \tag{2.4}$$

Based on the equation 2.4 the remaining unknown mass m_n was evaluated as [13]

$$m_n = 1.0067 \pm 0.0012 \text{ u}.$$

Current value of neutron mass given in Olive [14] resulting from improved and more accurate measurements of mass of the neutron, all based on Chadwick's technique, is

$$m_n = 1.0086649160 \pm 0.0000000004 \text{ u}.$$

This result matches remarkably well with Chadwick's results.

2.1 Basic Neutron Properties

Neutrons together with protons (collectively called nucleons) are particles that create atomic nuclei each consists of up-quarks and down-quarks. They reside in a nucleus bound together by the strong nuclear force. The up-quark has a charge of $+2e/3$ and the down-quark $-e/3$. Given the fact neutron consists of one up-quark and two down-quarks it has zero charge in total. In the view of fact that the neutron behaves like an elementary particle in neutron activation analysis, the quark model is not further concerned [7]. The basic properties of neutron are summarized in Table 2.1 (from Olive [14]).

Mass m_n	1.0086649160 u
Life time τ	880.3 s
Magnetic moment μ	-1.913 μ_N
Spin	1/2

Table 2.1: Elementary properties of neutron.

A neutron is to be bound in an atomic nucleus or free. A free neutron is not stable and decays spontaneously with a life time τ (see Table 2.1) into proton, electron and anti-neutrino through β decay

$$n \rightarrow \ p + e + \bar{\nu} + 0.782 \text{ MeV} \tag{2.5}$$

Such decay is possible due to the fact that the rest mass of proton plus electron is less than the rest mass of neutron. The kinetic energy that is released corresponds exactly to the difference between the rest mass of neutron and the sum of rest masses of the products. [1]

The neutron can be represented as either a wave with a certain wavelength λ_w, or a particle with a kinetic energy T, given in the units of electronvolts eV (de Broglie's wave-particle duality [5]). Depending on the velocity v of the particle the relationship for the wavelength

is

$$\lambda_w = \frac{h}{m_n v} \tag{2.6}$$

in which h is the Planck's constant. The corresponding kinetic energy is given by

$$T = \frac{h^2}{2m_n \lambda_w^2} \tag{2.7}$$

From equations 2.6 and 2.7 some assumptions follows. The lower the velocity of the free neutron, the longer the wavelength. If λ_w is much greater than the radius of a nucleus R_n ($\lambda_w \gg R_n$) the neutrons are called **thermal neutrons** with the energy about 0.025 eV. If the velocity of neutrons increases, the energy increases as well. Very high energetic neutrons (energy greater than 0.5 MeV) are refered as **fast neutrons**. [15]

A neutron source can produce neutrons with different range of kinetic energies. In most cases fast neutrons are produced. In order to obtain thermal neutrons, fast neutrons must be moderated by a low atomic mass material which decreases the velocity and hence the energy of fast neutrons to the thermal region. This process is called thermalization of fast neutrons. [13]

Neutron energy classification according to the kinetic energy of produced neutrons is following [11]

1. **Cold neutrons** $<$ 0.025 eV
2. **Thermal neutrons** $\sim$ 0.025 eV
3. **Epithermal neutrons** 0.025 eV $-$ 0.5 MeV
4. **Fast neutrons** $>$ 0.5 MeV

As seen above neutrons are generated over a wide range of energies by several processes leading to different types of interactions with nuclei. The first two categories are usually refered as slow neutrons because of the lower energy, hence lower velocity. Thermal neutrons with energy about 0.025 keV correspond to particles with velocity at the temperature 290 Kelvins. Epithermal neutrons are transition region between slow and fast neutrons showing often resonance behaviour when interacting with nuclei.

2.2 Interactions of Neutrons with Matter

This section concerns the basic interactions that occur when neutrons encounter matter. As the neutron lacks an electric charge, it is not attracted by the electromagnetic force between electrons and protons when it enters matter. The interactions of neutrons with matter are arranged through the strong force. This force is most effective within a short range of about 10^{-13} cm and therefore neutrons must come very close to the nucleus before anything can happen. [7]

The neutron can penetrate matter without any interaction or it can undergo a variety of nuclear interaction depending on its energy. These processes are

- **Elastic scattering** is a process during which the interacting neutron collides with a nucleus of a mass M that recoils with an angle ϕ with respect to the initial direction of motion of the neutron [16]. The kinetic energy of the neutron transfered to the nucleus is defined by the equation

$$T = \frac{4Mm_n}{(M+m_n)^2} cos^2\phi \tag{2.8}$$

  A derivation of Eq. 2.8 is provided by Bacon [17]. Neutron elastic scattering is the mechanism for slowing down fast neutrons, particularly by a medium with low atomic number. According to the Eq. 2.8 neutrons can transfer more energy to the low mass nuclei such as water (H_2O), heavy water (D_2O), graphite (C), and therefore materials from such nuclei are good moderators that slow down fast neutrons. [11]

- **Inelastic scattering** is an interaction at which the neutron is first scattered on the target nucleus leaving it in an excited state and then deflected with lower energy and different direction. The excited nucleus later decays by gamma-ray or some other form of radiation. Inelastic scattering occurs at the energy treshold on the order of 1 MeV and more. Below this treshold only elastic scattering occurs. [7]

- **Neutron Capture** is a reaction (n,γ) usually occuring at slow neutrons with high absorption cross section (see Section 2.3). The incident neutron is captured by the target nucleus and gamma-ray is irradiated away, for example

$$^{235}_{92}\mathrm{U} + n \rightarrow ^{236}_{92}\mathrm{U} + \gamma \tag{2.9}$$

  The final product is a compound nucleus in an excited energy state which undergoes gamma emission to go to the ground state [11]. This reaction describes the significant process used in **neutron activation analysis** which determines elemental composition of samples on the base of bombardment a sample with neutrons and subsequently detection of gamma-rays [18]. The subject of neutron activation analysis is treated in more detail in Chapter 3.

- **Other nuclear reactions** in which the incident neutron is also captured but charged particle is emitted, such as (n,p), (n,α), (n,2n), (n,d), etc [7]. Some of the reactions found use in neutron detection by interaction of neutrons with ^{3}He and ^{10}B

$$\text{(n,p)}: \ ^3_2\mathrm{He} + n \rightarrow ^1_1\mathrm{H} + ^3_1\mathrm{H} + 0.76 \text{ MeV} \tag{2.10}$$

$$\text{(n,}\alpha\text{)}: \ ^{10}_5\mathrm{B} + n \rightarrow ^7_3\mathrm{Li} + ^4_2\mathrm{He} + 2.8 \text{ MeV} \tag{2.11}$$

  These reactions produce either radioactive tririum or alpha particles. They become the secondary sources of ionization that can be detected to determine a neutron count rate. Other nuclear reactions with neutrons are also important in neutron activation analysis using fast neutrons which undergo these reactions. [11]

- **Nuclear fission** is an iteraction of neutron with fissionable nucleus. When a neutron interacts with such nucleus it becomes unstable and then fragments into two nuclides releasing more than one neutron and a high amount of energy at the same time. This

reaction found its important use in nuclear plants as sources of electrical power. [11]

The following section about cross section and reactions with neutrons gives clearer idea about how neutrons interact with matter.

2.3 Cross Section and Neutron Induced Reactions

The cross section refering to the probability for a nuclear reaction to occur is a measure of the effective size of a nucleus for a particular reaction. It is denoted by a greek letter σ and is defined as the number of reactions per unit time per nucleus divided by the incident intensity (number of incident particles per unit time per unit area) [1]. If $n(T)dT$ is the number of neutrons per unit volume having an energy between T and $T + dT$ and $\varphi(T)$ is the neutron flux defined as $\varphi(T) = n(T)v$ where v represents neutron velocity, then the number of neutrons giving the particular nuclear reaction (called reaction rate RR) in a material containing N nuclei is [19]

$$RR = N \int_0^{T_{max}} \varphi(E)\sigma_a(T)dT \tag{2.12}$$

in which T_{max} is the maximum kinetic energy of incident particles and σ_a denotes the cross section for a particular reaction a.

Cross sections are given in the dimensions of area of the order of the square of the nuclear radius or more convenient unit for cross section is **barn** (b) defined in [1] as following

$$1 \text{ barn} = 10^{-28} \text{ m}^2$$

Considering for example bombardment of carbon ^{13}C by protons, more cross sections are applied, each for a different nuclear reaction that occurs during the interactions, see Table 2.2 (from [1]).

Reaction	Interaction	Cross section
^{13}C(p,p)^{13}C	elastic scattering	σ_{pp}
^{13}C(p,p′)^{13}C*	inelastic scattering	$\sigma_{pp'}$
^{13}C(p,n)^{13}N	reaction (p,n)	σ_{pn}
^{13}C(p,γ)^{14}N	capture	$\sigma_{p\gamma}$
^{13}C(p,α)^{10}B	reaction (p,α)	$\sigma_{p\alpha}$

Table 2.2: Nuclear reactions that occur at bombardment of ^{13}C by protons.

The short notation ^{13}C(p,γ)^{14}N is often used as an abbreviating of a nuclear reaction

$$^{13}\text{C(p,}\gamma\text{)}^{14}\text{N}: \quad ^{13}\text{C} + p \rightarrow ^{14}\text{N} + \gamma. \tag{2.13}$$

Cross sections are defined for all kinds of nuclear reactions with photons, protons, neutrons, heavy ions, etc. Cross sections for nuclear reactions during which neutrons are involved, are so-called neutron cross sections. They differ within an energy of the incident

neutron. Neutron can be either scattered or captured by the interacting nucleus, dividing cross section into **absorption (capture) cross section** and **scattering cross section**. Thermal neutrons with energy about 0.025 keV are likely to be captured (absorbed) by the nucleus with the emission of γ ray from the excited nucleus. At low energies absorption cross sections tend to be inversely proportional to the velocity of neutrons $1/v$, the higher the velocity of the neutron, the lower the captured cross section. However, at intermediate energies (epithermal) cross sections often show sharp resonances for many elements. [13]

For fast neutrons the absorption cross sections are usually much lower in the comparison with the scattering cross sections. In Table 2.3 (cross sections from [20]) scattering and absorption cross sections are given with respect to thermal and fast neutrons for some elements. [21]

	Thermal σ (barn)		Fast σ (barn)	
Nuclide	Scattering	Absorption	Scattering	Absorption
^{1}H	20	0.2	4	0.00004
^{197}Au	8.2	98.7	4	0.08
^{16}O	4	0.0001	3	0.00000003
^{10}B	2	200	2	0.4
^{113}Cd	100	30 000	4	0.05
^{135}Xe	400 000	2 000 000	5	0.0008
^{115}In	2	100	4	0.02

Table 2.3: Thermal and fast cross sections for some nuclides.

Fast neutrons may undergo other nuclear reactions. These include (n,p), (n,α), (n,2n) accompanied by gamma-rays. These reactions are mostly threshold reactions. In other words, they can occur only above a given energy, characteristic for target nucleus. [21]

Fig. 2.1 gives an idea of some important nuclear reactions with neutrons and how the initial nucleus is shifted within the Karlsruhe Nuclide Chart. [2]

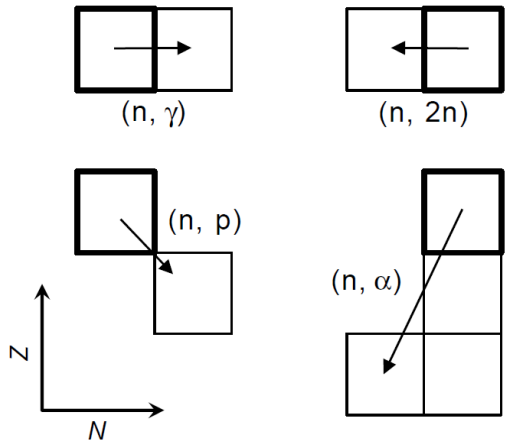

Figure 2.1: Some significant reactions with neutrons and shifts in Karlsruhe Nuclide Chart [2].

The left uppermost reaction is the radiative neutron capture and is a very important reaction for neutron activation analysis using thermal neutrons. The two reactions at the

bottom of Fig. 2.1 were already mentioned in Section 2.2 and their use in neutron detection was discussed. Reaction (n,2n) is only possible for fast neutrons used in neutron activation analysis using fast neutrons. [1, 2]

Summarizing, nuclear reactions with neutrons may be used for identification of isotopical composition of different kinds of target materials. Neutron activation analysis can be performed using various energy ranges of neutrons. The cross sections vary largely along the nuclide chart, hence neutron activation analysis show variable sensitivities for different elements. [21]

2.4 Neutron Sources

Many various types of neutron sources have been used to produce and apply neutrons using different methods of neutron production. As free neutrons are unstable particles decaying with half-life of approximately 10 minutes, they have to be released directly from nuclei. Radioisotopes, nuclear reactors and accelerator-based devices can be used as neutron sources. Radioisotopic way to produce neutrons is the use of bombardment of high energy radiation, such as gamma or alpha radiations, with low atomic number nuclei. Gamma and alpha radiations are usually obtained from other radioactive nucleus and these are cased in a low atomic mass elemental matrix. Some important nuclear reactions of this type [21] are listed below

1. Reaction (γ,n) with beryllium target produces neutron if the gamma-ray energy exceeds the neutron binding energy of a nucleus

$$\gamma + {}^{9}\mathrm{Be} \rightarrow 2^{4}\mathrm{He} + n - 1.67 \text{ MeV}$$

2. Neutrons are as well produced during reaction (α,n) when alpha particles bombard low atomic number isotopes

$$\alpha + {}^{9}\mathrm{Be} \rightarrow {}^{12}\mathrm{C} + n + 5.91 \text{ MeV}$$

Another way of producing neutrons is to use radioactive isotope which undegoes **spontaneous fission** during which it fragments into fission fragments along with the release of neutrons. The most common neutron source of such type is radioisotope Californium ^{252}Cf produced by irradiating uranium or another transuranic element in a nuclear reactor. Californium ^{252}Cf decays with a half-life of 2.65 years primarily by aplha emission (96.91 %) and the remaining 3.09 % decays by spontaneous fission producing average number of 3.7 neutrons per fission. [7, 11]

Nuclear fission is another way of producing neutrons which takes place within in a nuclear reactor that are used for power generation and experiments. When isotope of uranium, ^{235}U is exposed to slow neutrons, this results in the production of unstable ^{236}U which then splits into two fragments releasing neutrons and an average energy of 193.6 MeV [11].

The reaction may be illustrated by

$$^{235}\mathrm{U} + n \rightarrow \mathrm{fp} + k \cdot n + 193.6 \text{ MeV} \tag{2.14}$$

in which fp refers two fission fragments and $k = 2.42$ is an average number of neutrons released during the fission. The released neutrons are mostly fast neutrons thermalized by the surrounding moderator in the reactor. Thermal neutrons may be used for neutron activation analysis that uses radiative neutron capture. Nuclear reactors are widely used as neutron sources for experiments with generating neutron flux up to 10^{15} neutrons per $\mathrm{cm}^2\mathrm{s}$. Higher neutron fluxes reduce the time required to conduct the experiment. [21]

Neutron generator presents very low-power neutron source using deuterium and tritium as target materials according to the reactions ^{2}H(d,n)^{3}He and ^{3}H(d,n)^{4}He [22]

$$^2\mathrm{H} +^2 \mathrm{H} \rightarrow^3 \mathrm{He} + n + 3.29 \text{ MeV} \tag{2.15}$$

$$^2\mathrm{H} +^3 \mathrm{H} \rightarrow^4 \mathrm{He} + n + 17.6 \text{ MeV} \tag{2.16}$$

where the residual energy of the reaction, called Q value, is divided between the helium nucleus and the neutron. The fusion between deuterium and tritium (D-T reaction) gives rise to a 14 MeV neutron and the rest of the energy is transfered to the aplha particle (approximately 3.6 MeV). The energy of the neutrons can slightly vary because the energy depends on the angle at which the neutron escapes with repsect to the direction of motion of deuterium ion. Both the reactions are exothermic which implies low energy particle beams are requested. Neutron generators are sources of mostly monoenergetic neutrons and have found use in neutron spectrometry, neutron activation analysis, studying inelastic scattering of fast neutrons, etc. The significant advantage of neutron generator is the possibility to turn it off from the power source and the radiation stops immediately [21], [15].

Neutron generators are of great concern in this work and are treated in more detail in Chapter 5.

2.5 Protection from Neutron Radiation

Ionizing radiation effects a living tissue by ionization of neutral atoms the tissue consists of. Such effects lead to the danger of getting radiation sickness that may be fatal in some cases. The matter of public interest is to study radiation influence on the living tissue, radiation detection and of course protection. [3]

In planning neutron measurements it is important to know that interactions of neutrons may activate the surrounding material which then becomes a source of radiation as well. Since neutrons have no charge, they do not lose their energy so rapidly and can penentrate matter more easily. If a neutron interact with a nucleus, several nuclear reactions accompanied by strong gamma emission can take place. Wide range of half-lifes of activated material around a neutron source must also be taken into account. [13]

Shielding is required to protect people from harmful neutron and gamma radiation around neutron activation experiments. Fast neutrons as a source of protons (n,p) and alpha particles (n,α) can cause different kind of ionization as well. It is convenient to create a shielding that absorbs both neutrons and gamma-rays. Photons are strongly attenuated through lead shielding. Thermal neutrons are stopped by materials with high capture cross sections, such as cadmium, boron or lithium. In the case of cadmium the neutron capture is accompanied by strong gamma radiation so that lithium and boron are preferable materials because of lower gamma emission. Fast neutrons must be thermalized before being captured. For this heavy concrete is appropriate for shielding around neutron sources. Heavy concrete containing iron, hydrogen and boron combines all the features for slowing down and capturing neutrons. [13]

Chapter 3

14 MeV Neutron Activation Analysis

Nowadays neutrons are used in various fields of science and industry. Applications include among others elemental analysis, art and archeology, environmental and geological fields, electronics, medicine, biophysics, gas and oil industry [23]. Last decade of research and development presented a lot of neutron activation analysis applications in medical research, material non-destructive analysis (e.g. coal and cement), explosive detection, land mine detection, detection of contraband and threats in cargo and vehicles, security monitoring, etc. [24]

Neutron activation analysis (NAA) was developed by **G. Hevesy** and **H. Levi** in 1936 following the discovery of neutron by J. Chadwick in 1932. It has been demonstrated that induced radioactivity can be used for determining the presence of unknown elements in samples. The development of the method and its applications was defined by progress of its components such as nuclear reactors, neutron generators, scintillation detectors like NaI(Tl), the semiconductor detectors (Ge, Si), multichannel analyzers (MCA), computers and relevant software since the 1940s till today. [24]

NAA is a highly sensitive and efficient analytical method useful for performing both qualitative and quantitative analysis of a number of main components and trace elements in samples from almost every field of scientific or technical interest. In NAA [25] a sample is first irradiated with neutrons coming from e.g. a neutron generator or an experimental reactor. Depending on the neutron flux energy spectrum and reaction cross sections, the target nucleus undergoes a nuclear reaction and the resulting nucleus will immediately de-excite under emission of characteristic prompt gamma rays into a more stable configuration. This configuration is in general a radioactive nucleus with a certain half-life $T_{1/2}$ which will further decay under emission of characteristic delayed gamma rays into a stable product nucleus. Both prompt and delayed gamma rays are unique signatures of sample isotopical composition. The principle of function of neutron activation as elemental analysis is shown in Figure 3.1. NAA falls into two categories with respect to time and location of measurement as **prompt gamma neutron activation analysis** (PGNAA) and **delayed gamma neutron activation analysis** (DGNAA). PGNAA detects prompt gamma-rays com-

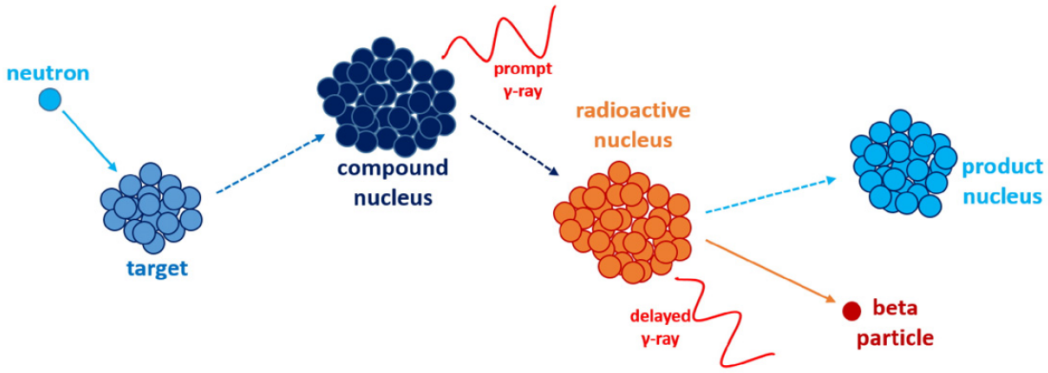

Figure 3.1: Principle of function of neutron activation as elemental analysis [18].

ing from a sample immediately after irradiation with neutrons. A sample, neutron source and gamma spectrometer must be placed close by in order to obtain prompt gamma-ray spectrum of activated sample. The PGNAA technique is applied in the cases when measurement by DGNAA is not the right option, e.g. elements decay too rapidly or delayed gamma-rays are of low intensities. DGNAA is applicable in most cases for the vast majority of elements producing radioactive nuclei. Gamma-ray detection of activated samples can be performed after irradiation with respect to half-lifes of formed radionuclides [18], [23]. PGNAA and DGNAA processes of activation and detection are illustrated in Fig. 3.2. It shows both thermal NAA and fast NAA. Thermal neutrons are created during 14 MeV NAA from fast neutrons which are slowed down via inelastic scattering in surrounding matter. Prompt gamma rays are usually emitted during inelastic neutron scattering (n,n'γ) and radiative neutron capture (n,γ). Other nuclear reactions, such as (n,α), (n,p), are mostly accompanied by delayed gamma-rays. When 14 MeV NAA being performed, fast neutrons

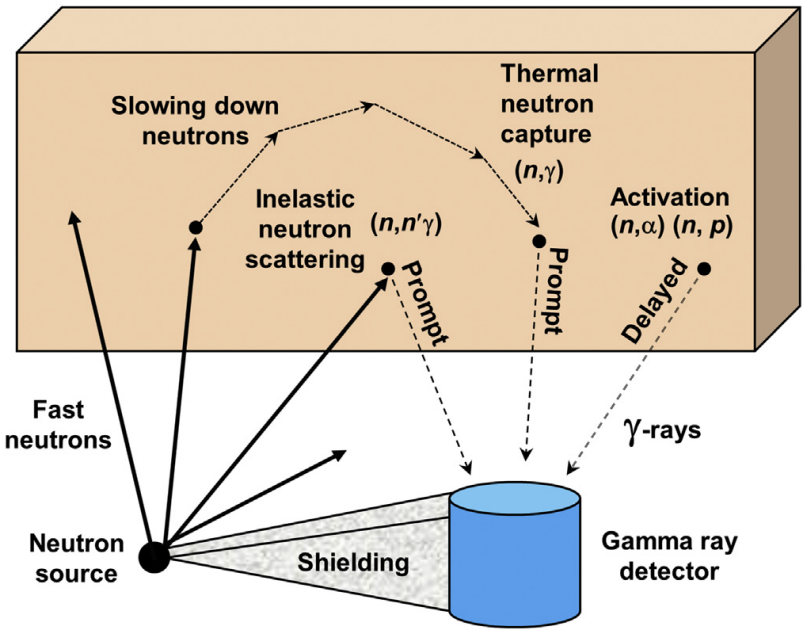

Figure 3.2: Illustration of prompt and delayed gamma neutron activation analysis [26].

may react with target nuclei through other than neutron capture reaction. Formed radionuclides usually end up in an excited state and release the redundant energy through gamma emission. Table 3.1 (data from [21]) lists some important reactions for 14 MeV neutron activation analysis. Both prompt and delayed gamma-rays are emitted during the reactions. Some limitations of this method may arise when an interference appears. Two different elements may form the same radioactive nucleus after irradiation with 14 MeV neutrons. In the table silicon and phosphorus undergo different nuclear reactions but form the same radionuclide, ^{28}Al decaying with the half-life of 2.25 min through emission of 1 780 keV gamma-ray. In some cases close-lying gamma peaks from different reactions can be detected as one peak if the energy resolution of gamma spectrometer is not more precise. Some other elements not present in the table may be well analyzed using this method: F, Mg, Fe, Zn, S, Yr, Mo, Br and Sn. Fig. 3.3 shows delayed gamma spectrum of plates

Element	Reaction	$T_{1/2}$	E_γ(keV)
Boron	^{11}B(n,p)^{11}Be	13.8 s	2125
Oxygen	^{16}O(n,p)^{16}N	7.13 s	6129
Nitrogen	^{14}N(n,2n)^{16}N	9.97 min	511
Aluminium	^{27}Al(n,p)^{27}Mg	9.46 min	844
Silicon	^{28}Si(n,p)^{28}Al	2.25 min	1780
Phosphorus	^{31}P(n,α)^{28}Al	2.25 min	1780
Copper	^{63}Cu(n,2n)^{62}Cu	9.74 min	511
Silver	^{109}Ag(n,2n)^{108}Ag	2.37 min	633
Baryum	^{138}Ba(n,2n)^{137}Ba	2.55 min	662

Table 3.1: Some important reactions of elements with 14 MeV neutrons.

measured by HPGe spectrometer after activation using 14 MeV neutron flux from D-T neutron generator. Spectrum shows significant peaks of gamma-rays emitted by the isotopes produced by neutron activation. The experiment was performed at VŠB-TU in Ostrava in 2011 [27]. Table 3.2 displays clearly identified neutron induced reactions in the gamma spectrum.

Reaction	σ (mb)	E_γ(keV)
^{27}Al(n,p)^{27}Mg	73	844
^{27}Al(n,α)^{24}Na	123	1015, 1367, 2754
^{28}Si(n,p)^{28}Al	280	1779
^{29}Si(n,p)^{29}Al	137	1273
^{56}Fe(n,p)^{56}Mn	114	847, 1811, 2113
^{124}Sn(n,2n)^{123}Sn	1515	160

Table 3.2: List of neutron induced reactions, cross-sections and gamma energies for gamma spectrum in Fig. 3.3.

It is possible to overcome the (n,n'γ) energy treshold and excite some of the widepsread elements, such as carbon, oxygen, nitrogen and sulphur, using the 14 MeV neutrons and prompt gamma-ray spectra may be obtained showing specific peaks representing isotopes of chemical elements in measured sample. The energies of prompt photons produced in de-excitaction of carbon, oxygen, nitrogen and sulphur during (n,n'γ) reaction are stated in Table 3.3. [28]

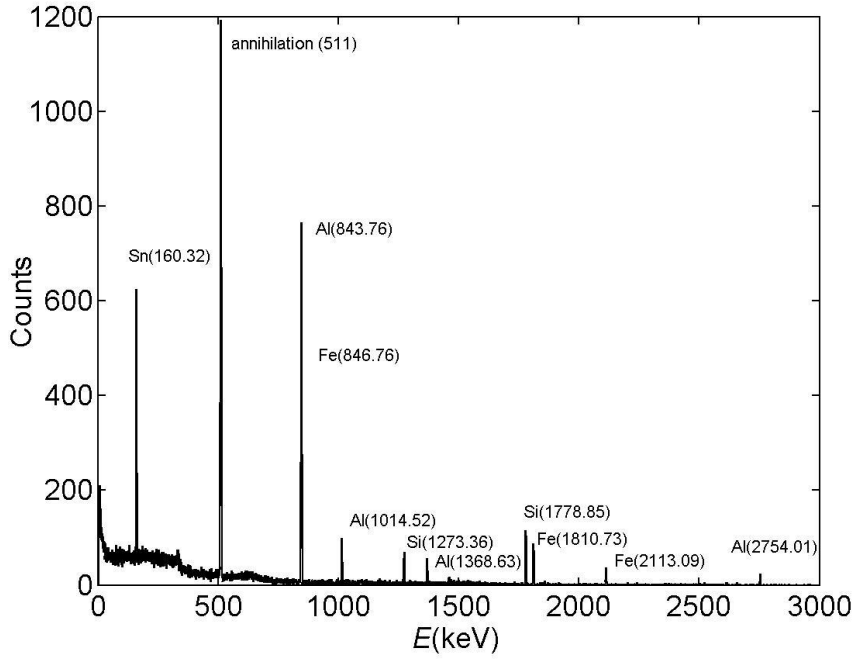

Figure 3.3: Delayed gamma-ray spectrum of sample plates irradiated by 14 MeV neutron flux from D-T neutron generator.

Isotope	E_γ(keV)
^{12}C	4400
^{16}O	6129.3
^{14}N	729.6, 2312.8
^{32}S	1273, 2230.2

Table 3.3: Prompt gamma-rays induced by 14 MeV neutrons during (n,n'γ) reaction.

With respect to sample chemical modification NAA falls into two categories according to whether radiochemical separations are done to samples after irradiation. If yes NAA is called **radiochemical neutron activation analysis** (RNAA). The method is able to remove interferences or concentrate the radioisotope of interest. Due to its high costs and difficulties this technique is performed infrequently. In majority of cases application of purely instrumental procedures is done as **instrumental neutron activation analysis** (INAA). It is one of the most important advantages of NAA over other analytical methods. The method analyzes samples without any chemical processing. INAA can process and analyze aerosol, ash, rocks, ores, minerals and some other types of material. [18]

3.1 Determination of Mass Using NAA

Induced radioactivity of a given isotope in a neutron activated sample is related to the mass of the element in the sample. Both absolute and relative NAA standardization modes are applied in order to calculate the mass of investigated element. The NAA mass measure-

ment method is based on calculating the mass either directly from the measured induced activity, so-called absolute method, or comparing the activity with the activity of a standard with known mass, called relative method. [19]

From the reaction rate Eq. 2.12 the mass m_A obtained from the knowledge of the neutron flux φ (the absolute method) and measured gamma spectrometry data, is derived in [29] as the following equation

$$m_A = C \cdot \frac{M_A}{N_{av} \cdot \theta} \cdot \frac{\lambda}{\varphi \cdot \sigma \cdot P_\gamma \cdot \varepsilon \cdot (1 - e^{-\lambda t_i}) \cdot e^{-\lambda t_d} \cdot (1 - e^{-\lambda t_m})} \tag{3.1}$$

in which

- m_A is the mass of the irradiated element in grams,
- C is the number of counts in the measured gamma peak of energy E_γ,
- N_{av} is the Avogadro's number in mol^{-1},
- M_A is the molar mass in $\mathrm{g \cdot mol}^{-1}$,
- θ represents the isotopic abundance of the target isotope,
- σ is the cross section for particular neutron induced reaction,
- P_γ is the probability of emission of a photon with energy E_γ,
- ε is the full-energy photopeak efficiency of the detector,
- t_i is the time of irradiation in seconds,
- t_d is the time of decay during transportation to a detector in seconds and
- t_m is the time of measurement in the detector in seconds.

The second way of determining the mass (m_R) is the relative method that is based on irradiation of an unknown sample together with a standard upon the same conditions containing known mass of the investigated element. The calculation of the mass of the element in an unknown sample is made according to the equation [29]

$$m_R = m_{ST} \cdot \frac{I_r}{I_{st}} \tag{3.2}$$

where I_R and I_{ST} are following

$$I_R = \frac{C}{(1 - e^{-\lambda t_i}) \cdot e^{-\lambda t_d} \cdot (1 - e^{-\lambda t_m})} \tag{3.3}$$

$$I_{ST} = \frac{C_{st}}{(1 - e^{-\lambda t_i}) \cdot e^{-\lambda t_d} \cdot (1 - e^{-\lambda t_m})} \tag{3.4}$$

A relative standardisation can be performed using standards prepared for the identification of elements by the means of neutron activation analysis.

3.2 Texas Convention Technique

The neutron flux needs to be determined in order to use it for calculation of mass using NAA or for neutron spectrometry measurements. The possible approach how to measure the intensity of a neutron flux, is to take into account certain neutron absorption reactions. These lead to the formation of radioisotopes and their induced activity can be measured by gamma spectrometer. Then the activity of an activated sample is directly related to the neutron flux. [30]

A thin copper foil of known physical and nuclear properties is used for neutron flux determination. The foil is irradiated by neutrons from a neutron source for a given time t_i, afterwards it is removed away from the source and transfered to a spectrometer that measures the activity of the foil. Two more times are needed to be measured, t_d as the time of transportaion of the foil to a gamma counter and t_m as the time of measurement in the counter. The nuclear reaction which takes place during the bombardment of copper foil with 14 MeV neutrons is (n,2n) reaction as following

$$^{63}\mathrm{Cu} + n \rightarrow ^{62}\mathrm{Cu} + 2n \tag{3.5}$$

The formed radioisotope of copper ^{62}Cu decays via β^+ decay with half-life of 9.74 min [10] releasing positrons. The foil is placed between two lucite absorbers inside which the positrons annihilate. It leads then to the creation of annihilation peak in gamma spectrum. The number of counts of annihilation peak measured on gamma counter is related with the neutron flux by following relation [30]

$$\varphi = \frac{n_t\ \sigma_t\ \lambda\ C}{\varepsilon\ b\ A\ n_p\ \sigma_{n2n}\ (1 - e^{-\sigma_t n_t x})\ (1 - e^{-\lambda t_i})\ e^{-\lambda t_d}\ (1 - e^{-\lambda t_m})} \tag{3.6}$$

in which

- φ is the neutron flux in cm^{-2}s^{-1},
- n_t represents the number of Cu nuclei per unit volume (cm^{-3}),
- σ_t is a total cross section in cm^2,
- λ is a disintegration constant of ^{62}Cu in s^{-1},
- C the number of counts of annihilation peak (511 keV),
- ε represents the full-energy peak efficiency for 511 keV plus the correction for self-absorption,
- b is the branching ratio expressing emission probability per one decay (two photons per decay),
- A is the area of the foil in cm^2,
- n_p is the number of ^{63}Cu nuclei per unit volume (cm^{-3}),
- σ_{n2n} refers the cross section for reaction ^{63}Cu(n,2n)^{62}Cu in cm^2,

- x is the foil thickness in cm,
- t_i is the time of irradiation in seconds,
- t_d is the time of transportation to gamma counter in seconds and
- t_m is the time of measuring the foil on gamma counter in seconds.

To obtain a neutron yield of a neutron source in the units of neutrons per second the neutron flux φ at the location of the copper foil is multiplied with the area of a sphere with the radius as the distance between the foil and the center of neutron production (target plane)

$$\varphi_0 = \varphi \, 4\pi r^2 \tag{3.7}$$

where φ_0 is the neutron yield of the neutron source and r stands for the distance between the target plane and the location of the foil.

3.3 Applications of 14 MeV neutron activation analysis

Neutron activation analysis performed using fast neutrons has many possible applications in various fields of interest. 14 MeV NAA is very sufficient in determining light elements such as oxygen, nitrogen and carbon, which are present in explosives and weapons. Pulsed 14 MeV NAA has been used in medical applications in body screening. The method can serve properly when investigating isotopes with high cross sections for 14 MeV neutrons. Overview of some existing applications with 14 MeV neutrons are surveyed below ([21])

1. Explosives detection in security: cargo/luggage inspection, suspisious objects with content of C, O, N.
2. Chemical weapon detection: N, P.
3. Contraband detection: narcotics, C, O, N.
4. Art and archeology: major components detected by thermalized 14 MeV neutrons (big advantage: the method is non-destructive for the artefacts and archeological objects).
5. Industrial applications: metal cleanliness (oxygen in Mg, Al, Steel).
6. Medical applications: body screening using pulsed 14 MeV (C, O, N, Ca, Na, Cl, P).
7. Protein content of food in nutrition: content of nitrogen.
8. Applications in environment: detection of halogens (fluorine content).

Neutron activation analysis finds a great usage in classifying threats, such as weapons, explosives, narcotics and other possible risks. In [31] it was presented a 14 MeV neutron interrogation system alowing the detection of threats in hidden compartments of maritime vessels. The system consists of a neutron generator, a gamma spectrometer and a data aquisition computer. Elements are identified by analyzing prompt gamma-rays induced by the

neutron activation. According to the elemental composition of common substances, narcotics, explosives and chemical weapons, the classification of the threats can be performed with this system. Each threat has different signatures in elemental compositon.

Another significant usage of 14 MeV NAA is in heavy oil production control. In [32] possible approaches were published concerning how to use neutron interrogation methods in oil production control. Due to good penetration of neutrons the masurements can be made through the pipe walls, the devices can be easily installed without interruption of the production process. NAA allows determination of oil content by measurement of major components in oil, such as hydrogen, carbon, oxychen, chlorine, sulphur, etc. It is also possible to use NAA to measure flow rate without interruption. The fluid in the conduit is bombarded with neutron pulses activating isotopes in the fluid. The activated isotopes decaying with the variety of half-lifes are transported with the flow and the released gamma-rays can be detected downstream providing the information about the velocity.

Chapter 4

Calibration of NaI(Tl) Scintillation Spectrometer

We performed our NAA measurements of activated samples on NaI(Tl) scintillation spectrometer made by Canberra Industries, Inc [33]. Using this spectrometer we collected gamma spectra from neutron flux measurements (Section 5) and samples activated with 14 MeV neutrons (Section 6). In order to obtain precise data from NAA measurements energy and efficiency calibrations of the spectrometer were established.

4.1 Description of NaI(Tl) Scintillation Spectrometer

The gamma spectrometer consists of scintillation crystal from natrium iodide doped with thallium. The crystal is of cylindrical shape with 3″ in diameter and 3″ in length. The crystal is covered with 2 mm thick reflector and closed in 0.5 mm thick alluminium housing (scheme of the spectrometer in Fig. 4.6) and joined to a photomultiplier on one side that converts the light into electrons. The spectrometer is connected to multi-channel analyzer MCA that is connected to a computer with GENIE 2000 basic spectroscopic software a comprehensive environment for data acquisition, display and analysis of gamma spectrometry data. Fig. 4.1 shows NaI(Tl) spectrometer placing in the Laboratory for Neutron Activation Analysis and Gamma Spectrometry in Ostrava. The spectrometer is enclosed in 10 cm lead shielding with two inner 1 mm thick Cd and Cu liners.

4.2 Energy Calibration

To determine the relationship between the channels of MCA and corresponding gamma energy we measured a gamma spectrum of ^{60}Co releasing two gamma-rays with energies approximately $\gamma_1 = 1173.2$ keV and $\gamma_2 = 1332.5$ keV. There is a third significant peak in the spectrum resulting from coincidence of γ_1 and γ_2 as their sum. The spectrum of ^{60}Co is shown in Fig. 4.2.

Figure 4.1: Lead shielding of the spectrometer (left), NaI(Tl) spectrometer in lead shielding (middle) and detail of NaI(Tl) crystal in an aluminium housing (right).

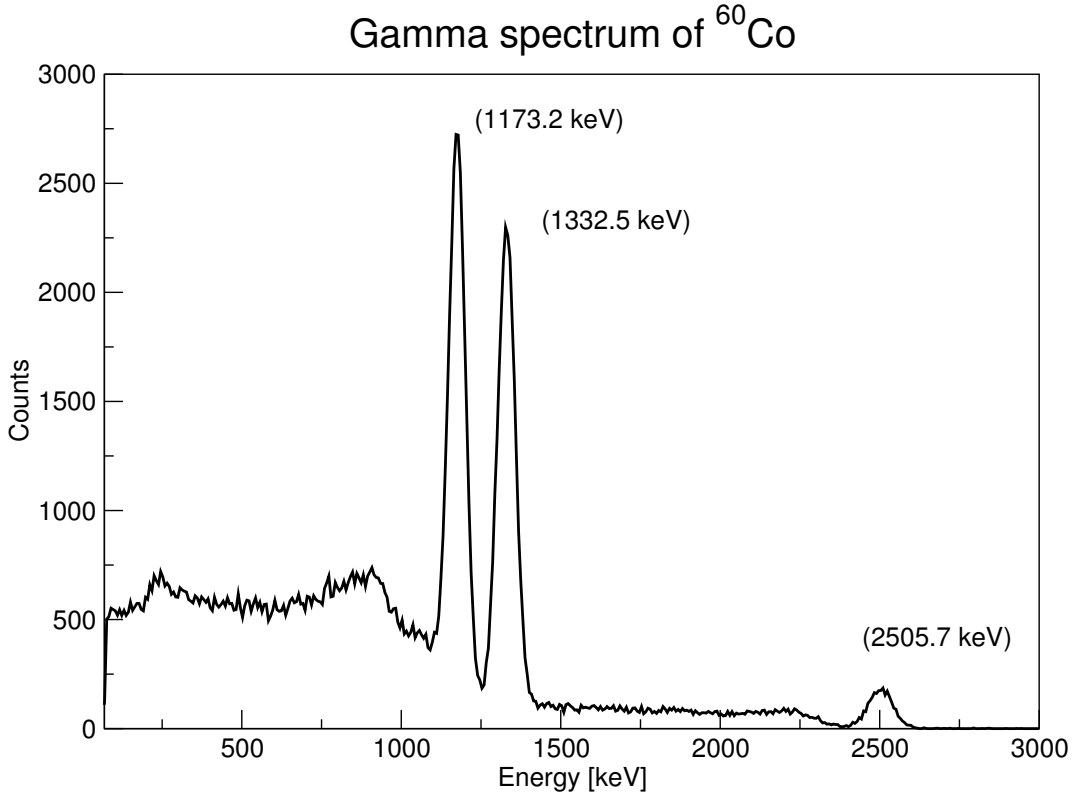

Figure 4.2: Gamma spectrum of ^{60}Co.

The three peaks were used to calculate the energy calibration equation using the channel positions of the measured gamma-rays in the spectrum and the real gamma-ray energies. Table 4.1 contains gamma-ray energies after calibration, the corresponding channels and the real gamma-ray energies of ^{60}Co. According to the results in Table 4.1 we can assume the energetic resolution of the scintillation spectrometer is accurate.

Channel	E_γ (keV) after cal.	Real E_γ (keV)
174.42	1176.63	1173.237
197.64	1333.45	1332.501
371.37	2512.23	2505.738

Table 4.1: Spectrometry data of ^{60}Co used for energy calibration of NaI(Tl) spectrometer.

Using function "Energy Only Calibration" in GENIE 2000 (see Fig. 4.3), we determined the energy calibration function as following

$$E(\text{keV}) = -4.95(\text{keV}) + 6.761 \cdot Ch \tag{4.1}$$

where Ch stands for a channel and E for the corresponding energy. Using the Eq. 4.1 we are able to achieve a good energy resolution in gamma spectrometry measurements and distinguish gamma energies of peaks in gamma spectra. The energy calibration accuracy was verified by displaying gamma energies released by ^{152}Eu along the approximate function (Fig. 4.3). ^{152}Eu is a multi-energetic gamma source which is used as an energy calibration source as well. Its spectrum can be found in Appendix A.

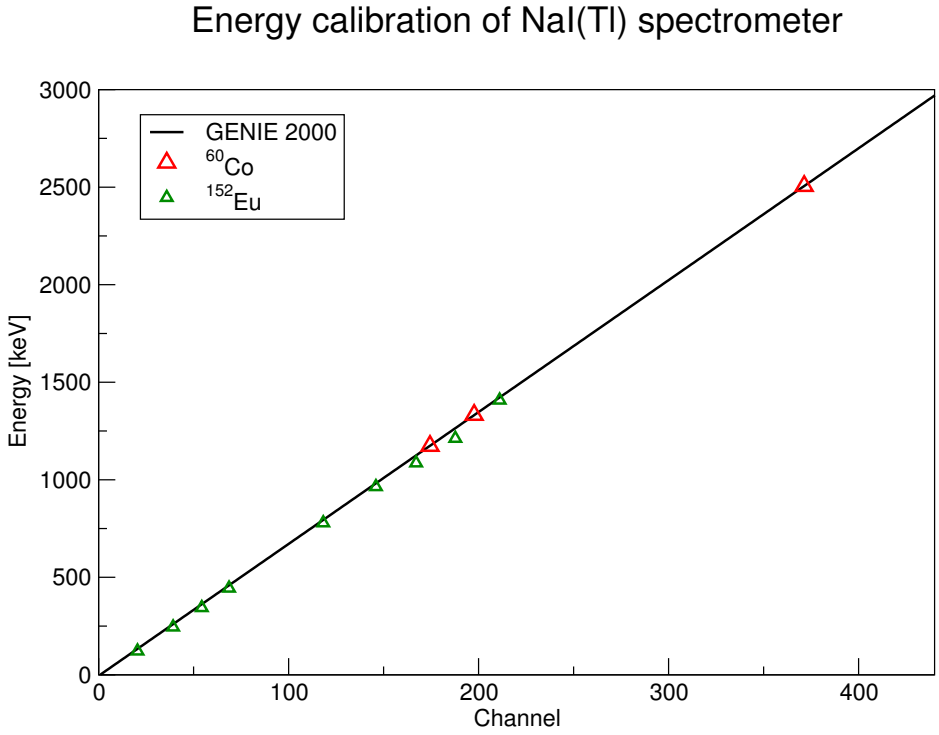

Figure 4.3: Energy calibration obtained using the gamma spectrum of ^{60}Co (red triangles), data interpolated using GENIE 2000 (black line) and the energy calibration function verified by ^{152}Eu (green triangles).

The energy calibration equation has a linear tendency. The relation was used to assign the gamma energy to the particular channel in order to distinguish gamma peaks in the most proper and suitable way.

4.3 Efficiency Calibration

Efficiency calibration provides the relationship between the energy of detected gamma-ray and the efficiency of detection. As mentioned in Section 1.3.3 the efficiency curve for a spectrometer shows non-linearity and strongly depends on the energy of gamma-ray being detected. The spectrometer efficiency is also influenced by the structure and dimensions of the spectrometer, geometry of measured gamma source and its distance from the spectrometer cap. In order to calculate efficiency curve for NaI(Tl) spectrometer in our case we proceeded by two different approaches to confirm the efficiency accuracy.

First approach we used was experimental. We measured gamma spectra of selected point monoenergetic gamma sources (summarized in Table 4.2) with known activity spreading over wide energy range. The point gamma sources were located in 1.5 mm distance from the spectrometer. We calculated the efficiency for each gamma energy released by the sources using the Eq. 1.16. The energy intervals between the chosen gamma energies were approximated using a suitable function in software GENIE 2000.

Radioisotope	E_γ (keV)	A_0 (kBq)	$T_{1/2}$ (days)	P_γ	Reference date
^{57}Co	122.13	154.1 ± 0.62	271.79	0.856	25.6.2014
^{137}Cs	661.67	90.04 ± 0.54	11019.35	0.851	15.9.2014
^{54}Mn	834.07	454.8 ± 3.64	312.03	0.999	25.6.2014
^{65}Zn	1114.64	206.1 ± 1.03	243.66	0.506	25.6.2014

Table 4.2: Spectrometry data of monoenergetic gamma sources used for efficiency calibration of NaI(Tl) spectrometer.

Activity A_0 is related to the reference date found in the certificate of the particular gamma source. Activity A related to the date of measurement 28.4.2017 was calculated using the Eq. 1.5 summarized in Table 4.3.

Radioisotope	A (kBq)
^{57}Co	12.59 ± 0.05
^{137}Cs	85.08 ± 0.51
^{54}Mn	51.34 ± 0.41
^{65}Zn	12.61 ± 0.06

Table 4.3: Activities of gamma sources calculated for date of measurement 28.4.2017.

The selected gamma sources were measured on NaI(Tl) spectrometer using GENIE 2000 software. Measured spectrometry data (number of counts in the peak C and time of measurement t_m) are summarized in Table 4.4.

Radioisotope	C	t_m(s)
^{57}Co	1215823 ± 1215	432.14
^{137}Cs	2261399 ± 2261	229.24
^{54}Mn	1318458 ± 1318	253.15
^{65}Zn	164635 ± 439	331.61

Table 4.4: Spectrometry data for gamma sources evaluated in GENIE 2000.

The efficiencies for given energies were determined in accordance to the relation (1.16) and the measured data. The obtained values of efficiency are summarized in Table 4.5 and displayed in Figure 4.4.

Radioisotope	E_γ (keV)	Efficiency ε
^{57}Co	122.13	0.3019 ± 0.0013
^{137}Cs	661.67	0.1368 ± 0.00084
^{54}Mn	834.07	0.1152 ± 0.00093
^{65}Zn	1114.64	0.0915 ± 0.00050

Table 4.5: Values of efficiency for given gamma energies and their relative uncertainities.

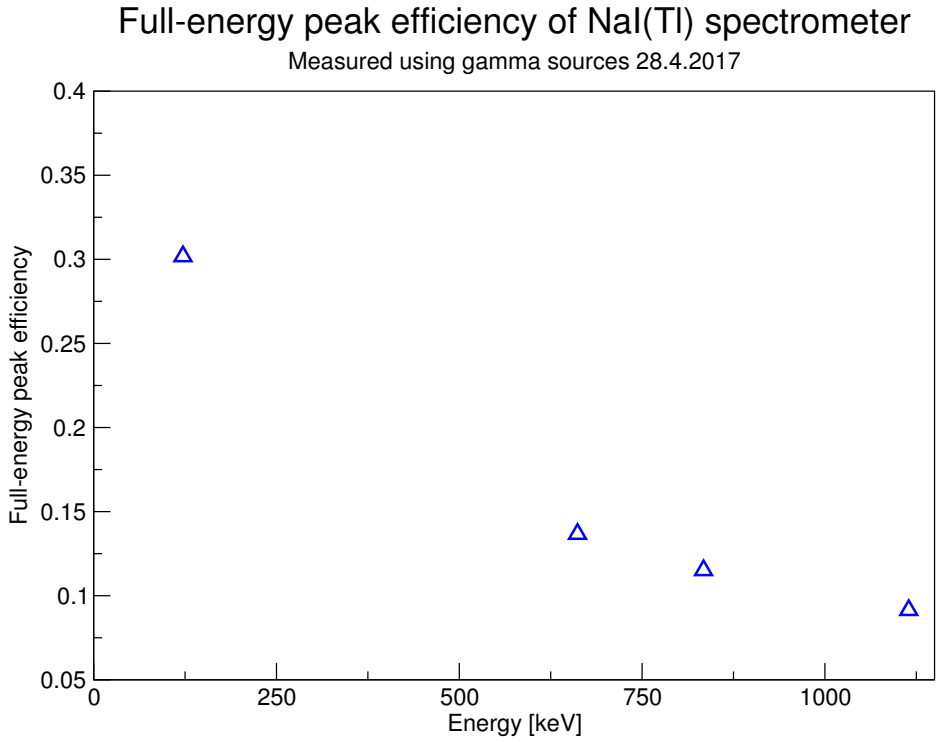

Figure 4.4: Full-peak energy efficiency of NaI(Tl) detector calculated using monoenergetic gamma sources from Table 4.2.

GENIE 2000 can determine the efficiency equation and curve straight from entering the values of efficiency calculated from our measurement as shown in Table 4.5, and by fitting the values using the right approximation function. The following equation represents the efficiency function for NaI(Tl) spectrometer calculated from the measured efficiency

values

$$ln(\varepsilon) = -3.193 + 1.069 \cdot ln(E) + 0.136 \cdot ln(E)^2. \quad (4.2)$$

In Figure 4.5 the approximate efficiency function fits the measured values and allows us to determine the efficiency for every energy lying between approximately 122 keV to 1115 keV.

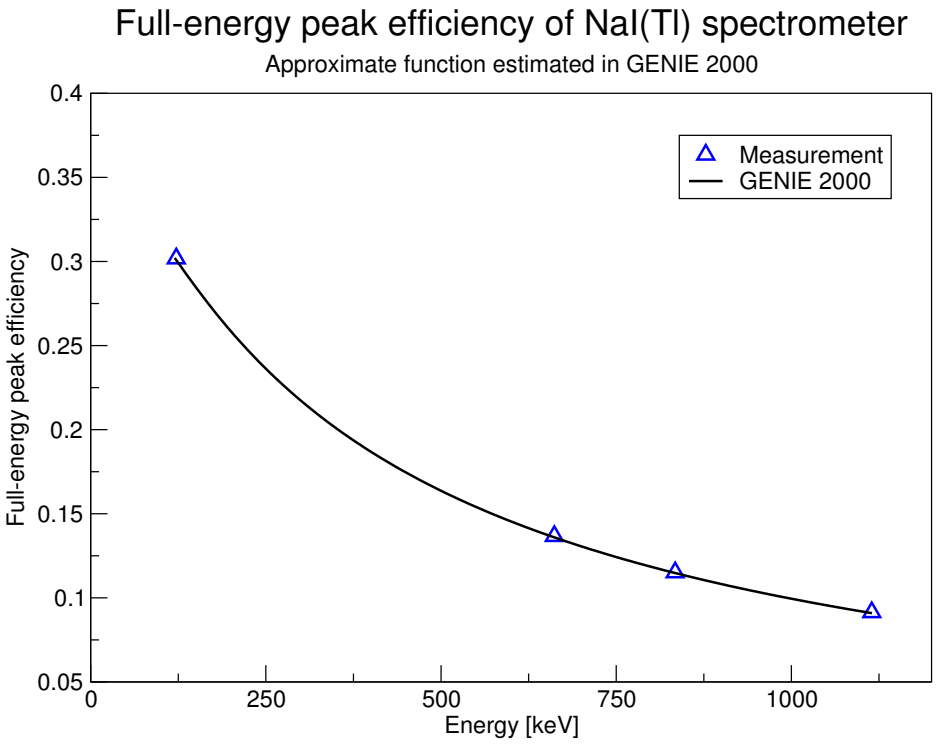

Figure 4.5: Full-peak energy efficiency curve for NaI(Tl) approximated using values from measurement approximated in GENIE 2000.

The second approach we followed to obtain efficiency function for NaI(Tl) spectrometer was a simulation run in a software called SpectraLineGP. The software is equipped with an efficiency calibration program that is able to determine the efficiency for scintillation and semiconductor spectrometers if all the partilular dimensions and materials of the spectrometer are known.

SpectraLine Gamma Precision (GP) [34] tool is a gamma analysis software that has been developed for wide range of application tasks in gamma spectrometry. The software contains among other features the calibration by efficiency and it allows the construction of approximate efficiency curves.

By running the simulation using the model of our NaI(Tl) spectrometer and the point gamma source in 1.5 mm distance from the spectrometer surface the efficiency function can be easily determined. The model of the spectrometer (Figure 4.6) was created in SpectraLineGP according to the real dimensions and materials provided by the manufacturer. The approximate efficiency curve determined in SpectraLineGP tool is displayed in Figure 4.7. The curve expresses the relationship between the efficiency and the energy ranging from 50 keV to 1200 keV. Using the function "calculate efficiency" in SpectraLineGP we are able

to obtain efficiency for every energy lying between the mentioned energy interval.

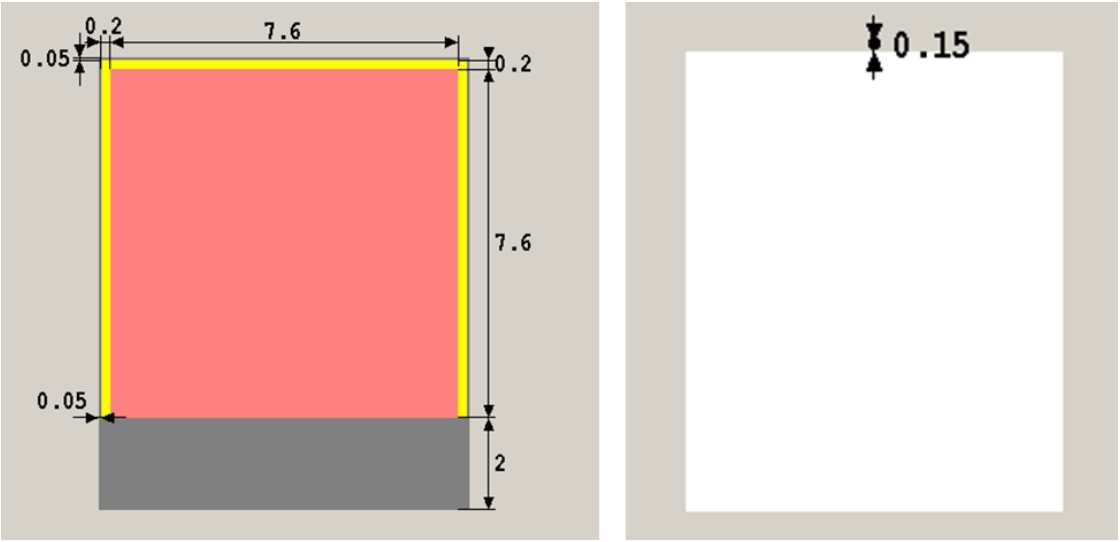

Figure 4.6: Model of NaI(Tl) spectrometer: 3″ x 3″ NaI(Tl) crystal (red) covered with 0.2 cm thick reflector from Al_2O_3 (yellow) and enclosed in 0.05 cm thick aluminium housing (grey), the aluminium mounting of the crystal is 2 cm thick. The point gamma source is located in 0.15 cm from the detector surface.

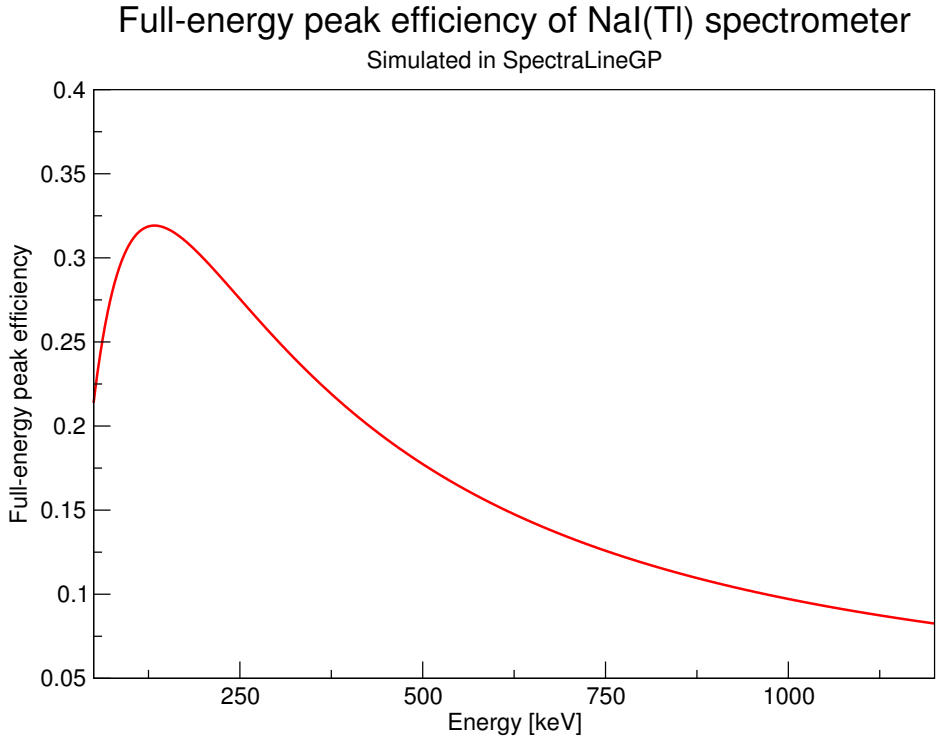

Figure 4.7: Full-peak energy efficiency of NaI(Tl) detector simulated by SpectraLineGP.

To determine the applicability of the approximate efficiency function estimated using the simulation in SpectraLineGP the efficiencies for the four point gamma sources are compared with the efficiencies calculated using the approximate efficiency function from Spec-

traLineGP in Table 4.6.

Radioisotope	E_γ (keV)	ε (measurement)	ε (simulation)
^{57}Co	122.13	0.3019 ± 0.0013	0.3065 ± 0.0059
^{137}Cs	661.67	0.1368 ± 0.00084	0.1406 ± 0.0040
^{54}Mn	834.07	0.1152 ± 0.00093	0.1138 ± 0.0036
^{65}Zn	1114.64	0.0915 ± 0.00050	0.0904 ± 0.0032

Table 4.6: Comparison of the measured and simulated values of efficiency.

Two methods of determining the efficiency curves of NaI(Tl) spectrometer were presented above. The first method was based on the measurement of four point gamma sources with known activity which enabled the direct calculation of the efficiencies for the given gamma energies. Approximate efficiency function was then found between these four points using the software GENIE 2000. The second method consisted of simulation in SpectraLineGP estimating the approximate efficiency function for the spectrometer using it properties (dimensions, construction material, distance between the point source and the detector cup).

The approximate efficiency curve obtained in SpectraLineGP is displayed in Figure 4.8 along with the values from the measurement of the efficiencies for the selected point gamma sources. We can notice the measured efficiencies lie nearly on the SpectraLineGP efficiency curve which confirms tha accuracy of the simulated efficiency curve and it can be used for calculating activities of point gamma sources releasing gamma-rays between 50 keV to 1200 keV.

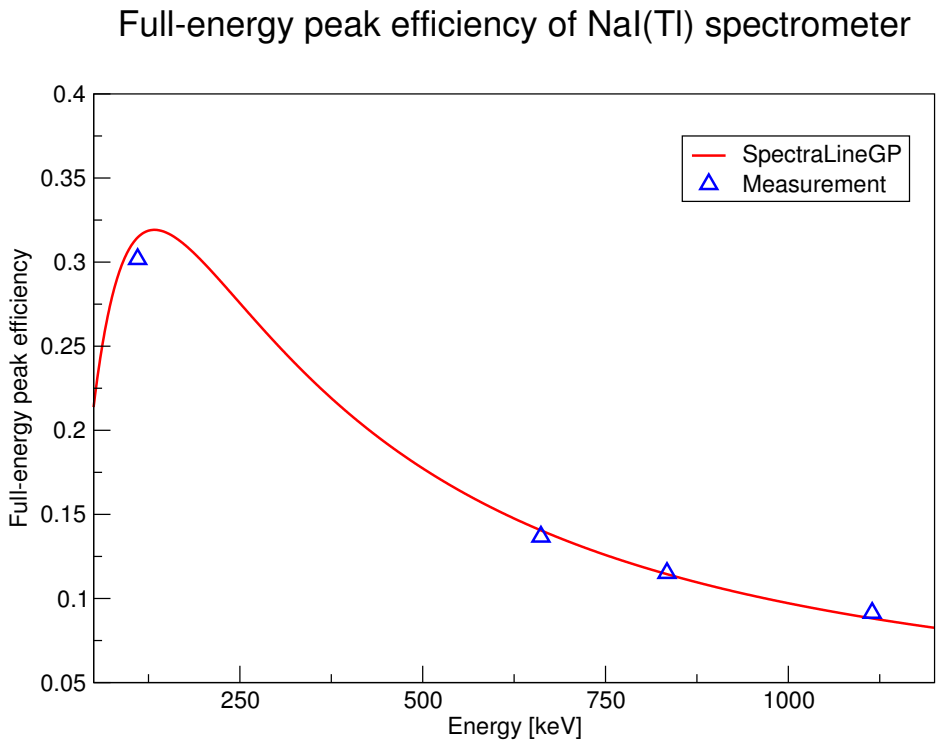

Figure 4.8: Full-energy peak efficiency of NaI(Tl) detector for both methods.

To determine efficiencies for gamma sources with other than point dimensions, we can easily simulate efficiency curves in SpectraLineGP for different types of sources, such as cylindrical shape or Marinelli beaker (Fig. 4.9).

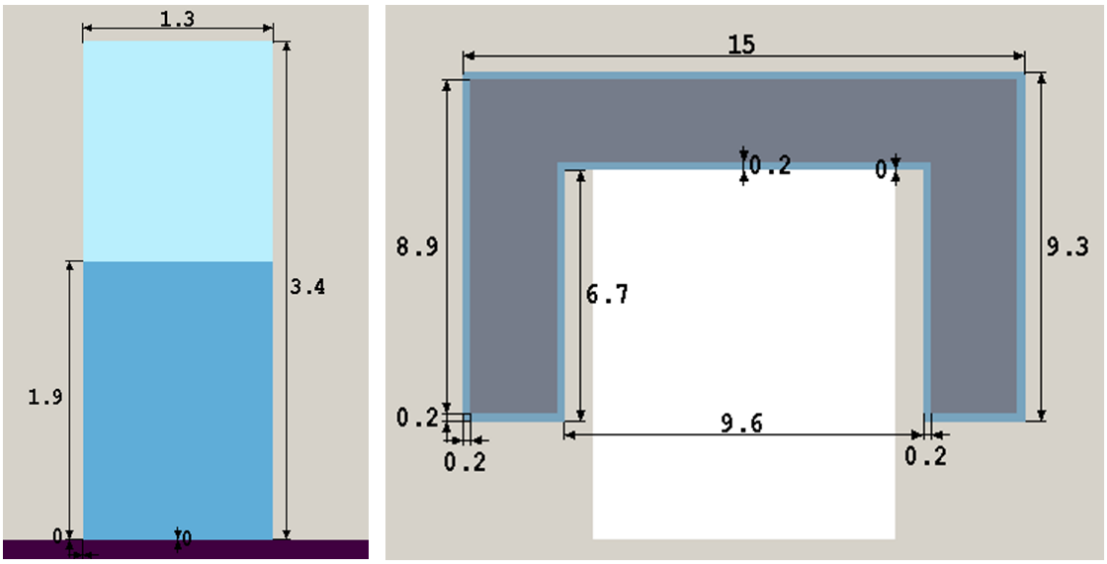

Figure 4.9: Different source shapes and geometries possible to use in simulations in SpectraLineGP to calculate efficiency curves. Dimensions are in centimeters.

Chapter 5

Calibration of Thermo Fisher Scientific MP 320 Neutron Generator

A neutron flux experiment was performed in order to obtain neutron generator calibration that is based on determining the real neutron flux and neutron yield of the neutron generator. Texas convention technique [30] was applied to calculate neutron flux in which a thin copper foil was irradiated by 14 MeV neutrons leading to a neutron absorption reaction producing positron emitter ^{62}Cu. The activity of ^{62}Cu can be measured by gamma spectrometer and is directly related to the neutron flux which formed the radioisotope ^{62}Cu. We followed this technique to determine the real neutron flux of MP 320 Neutron Generator (NG).

5.1 MP 320 Neutron Generator

The portable MP 320 neutron generator [35] produces 14 MeV neutrons from Deuterium-Tritium fusion, its maximum neutron yield reaches approximately 10^8 neutrons/s. It can operate in pulsed and continuous regimes and has a very low power consumption of less than 50 Watts. Typical tube lifetime is around 1200 hours at 10^8 n/s. The machine can be used for fast neutron activation analysis applied to detect explosives, buried land mines, chemical weapons, drugs, unexploded ordnance (UXO) detection, it can be used for elemental analysis of bulk metarials (coal, cement), mineral mining and exploration. Methods of material analysis are inelastic scatteriing, thermal neutron capture and delayed activation. Both prompt and delayed gamma spectra can be measured.

Technical specifications of Thermo Fisher Scinetific MP 320 NG are summarized in Table 5.1. The frequency of the deuterium pulses can range from 250 Hz to 20 kHz. Duty factor represents a fraction of a period in which the neutron generator produces neutrons. E.g. 10% duty factor means that the neutrons are produced 10% of the pulse time but 90% of the neutron pulse generation of neutrons is off. Duty factor of 100% means continuous regime.

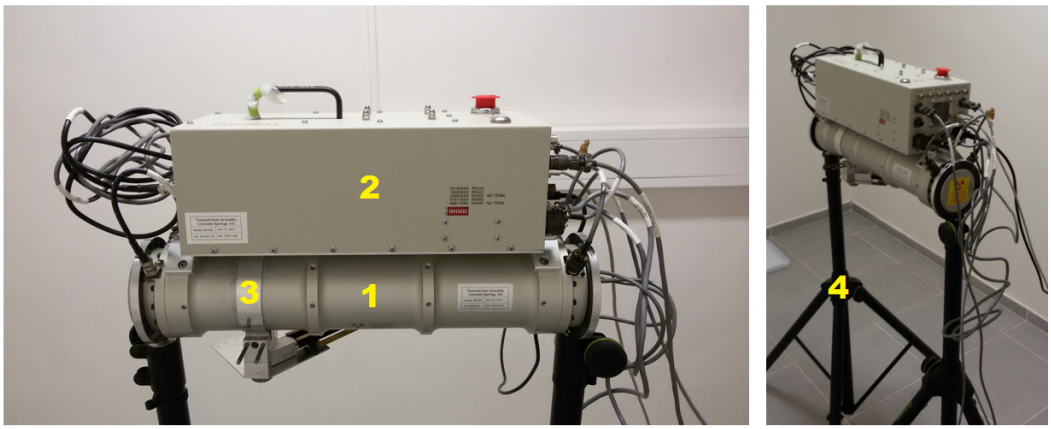

Figure 5.1: Thermo Fisher Scientific MP 320 neutron generator, (1) Accelerator tube, (2) Electronics case, (3) Target plane, (4) NG mounting.

The generator operates at maximum voltage 95 kV at which neutron yield higher than 10^8 n/s can be generated but higher neutron yield decreases the lifetime of the generator. The machine is operated remotely in open source text using commands or GUI interface on a computer. The NG electronics case was tested against radiation for 80 000+ hours.

Neutron Yield	10^8n/s (at 80 kV)
Neutron Energy	14 MeV
Typical Lifetime	1200 hours at 10^8n/s
Pulse rate	250 Hz to 20 kHz, continuous
Duty Factor	5% to 100%
Maximum Acceleration Voltage	95 kV
Beam Current	60 μA
Safety Features	Keylock, emenrgency button
Total Weight	12 kg

Table 5.1: Technical specifications of MP 320 NG.

5.2 Copper Foil Activation Experiment

We followed the Texas convention technique in order to obtain the real value of neutron flux and neutron yield of MP 320 NG. With the precise value of the neutron flux we are able to perform more accurate NAA measurements or the generator can serve as a calibration tool for neutron detectors since it is the source of almost monoenergetic neutrons. The knowledge of neutron flux is also needed for NAA measurements if absolute method of mass determination is used (see Eq. 3.1). We activated 0.775 mm thick copper foil with 14 MeV neutrons for a given experimental setup of the neutron generator and the foil. Basic parameters of the copper foil used for flux measurement are summarized in Table 5.2.

Gamma energy of ^{62}Cu decay	511 keV
Half-life	584.4 s
Decay constant	0.001186 s^{-1}
Diameter	2.5 cm
Thickness	0.775 mm
Number of Cu nuclei	$8.49 \cdot 10^{22}$ cm^{-3}
Number of ^{63}Cu nuclei	$5.87 \cdot 10^{22}$ cm^{-3}
Total cross section	$2.88 \cdot 10^{-24}$ cm^2
Branching ratio	1.94

Table 5.2: Basic parameters of copper foil used for neutron flux measurement.

The neutron generator was set on the voltage 80 kV, the beam current 60 μA, 10% duty factor and the frequency 1 kHz. The copper foil was placed at the angle 130° with respect to the direction of accelerated deuterium ions (see the scheme in Fig. 5.2) and in the distance 17.2 cm with respect to the target plane. The foil was irradiated for 600 seconds (t_i), transported to the counter for 180 seconds (t_d) and measured for 700 seconds (t_m). Spectrometry data obtained from activated copper foil are summarized in Table 5.3.

Number of counts C	11025 ± 132
Irradiation time t_i	600 s
Transportation time t_d	180 s
Measurement time t_m	700 s

Table 5.3: Spectrometry data obtained from the activated copper foil.

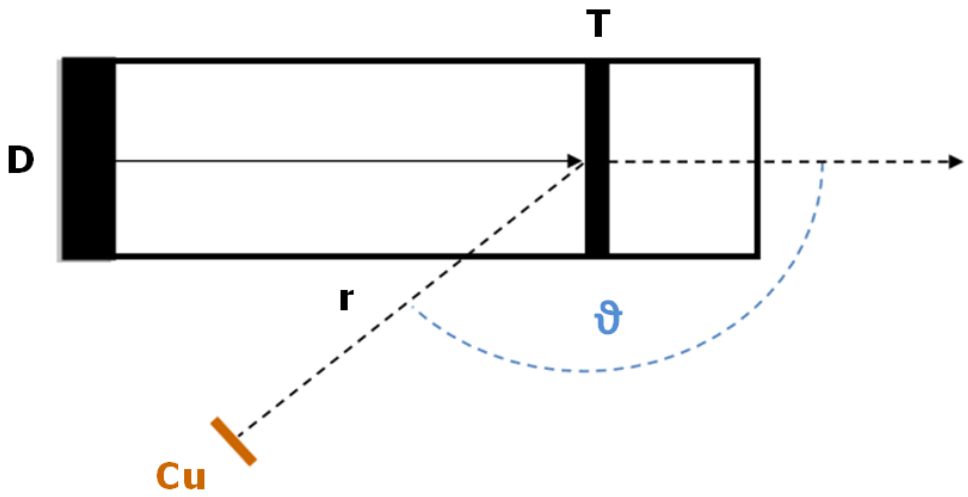

Figure 5.2: Scheme of the placement of the copper foil at an angle ϑ and distance r.

The copper foil measurement is displayed in Fig. 5.3. First the foil is prepared to be held in a proper holder. Afterwards the foil is irradiated upon an adjusted neutron generator setup. After the foil is activated, it is placed between two lucite cylinders (each 2.5 x 0.95 cm) for positrons to be annihilated and the annihilation 511 keV gammas are measured on the scitillation counter. The contribution of gamma-rays to annihilation peak can be

determined. The two lucite cylinders become the source of annihilation photons, this needs to be taken into account during efficiency calculation.

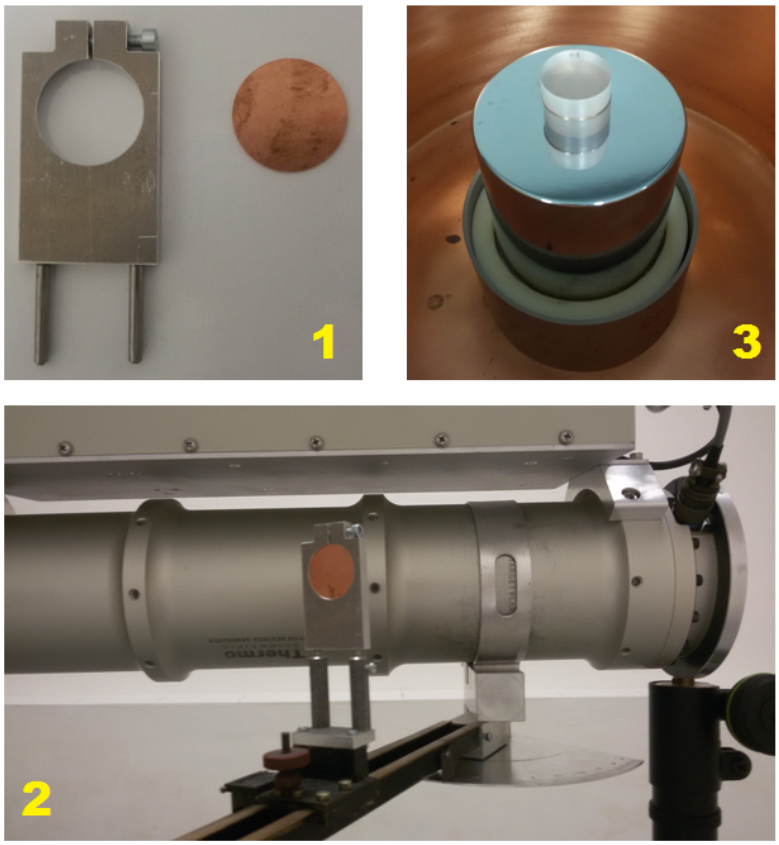

Figure 5.3: Copper foil preparation to a proper holder (1), neutron activation at an angle and a distance with respect to the accelerator tube and the target plane (2) and measurement of gamma spectrum on scintillation counter (3).

5.3 Spectrometer Efficiency for Copper Foil Activation Measurement

The activated copper foil was measured on NaI(Tl) spectrometer for which the efficiency function for point source was determined in Section 4.3 using the SpectraLineGP software and running a simulation. To obtain an efficiency function for a copper foil measurement we can use the same model of the spectrometer (Fig. 4.6) and as the source of annihilation photons we now use the geometry of a cylinder consisting of two lucite cylinders neglecting the thickness of the copper foil seen in Fig. 5.4.

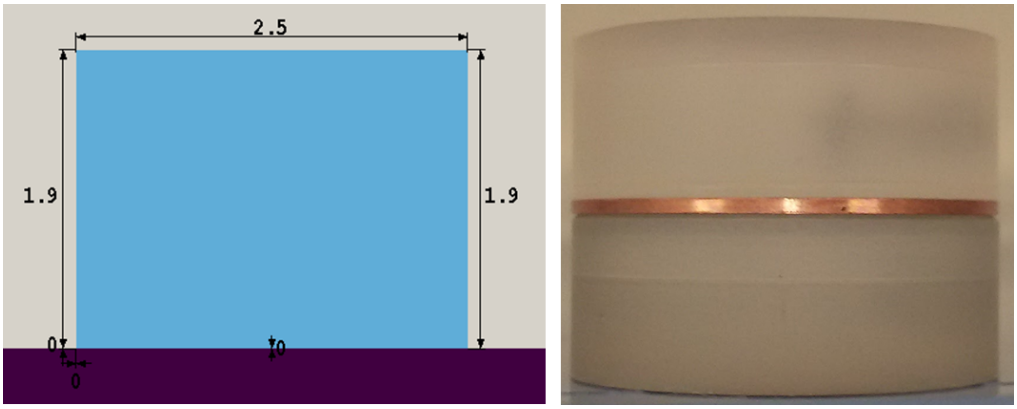

Figure 5.4: Model of the source of annihilation photons as the copper foil placed in two lucite cylinders, the thickness of the foil is neglected (left), the real source of annihilation photons (right).

By running the simulation in SpectraLineGP and using the approximate source geometry we obtain the approximate efficiency function from 50 keV to 1200 keV (Fig. 5.5). Using the function "calculate efficiency" we get the efficiency for measured energy 511 keV that is needed for neutron flux determination:

$$\varepsilon = 0.1133 \pm 0.0036.$$

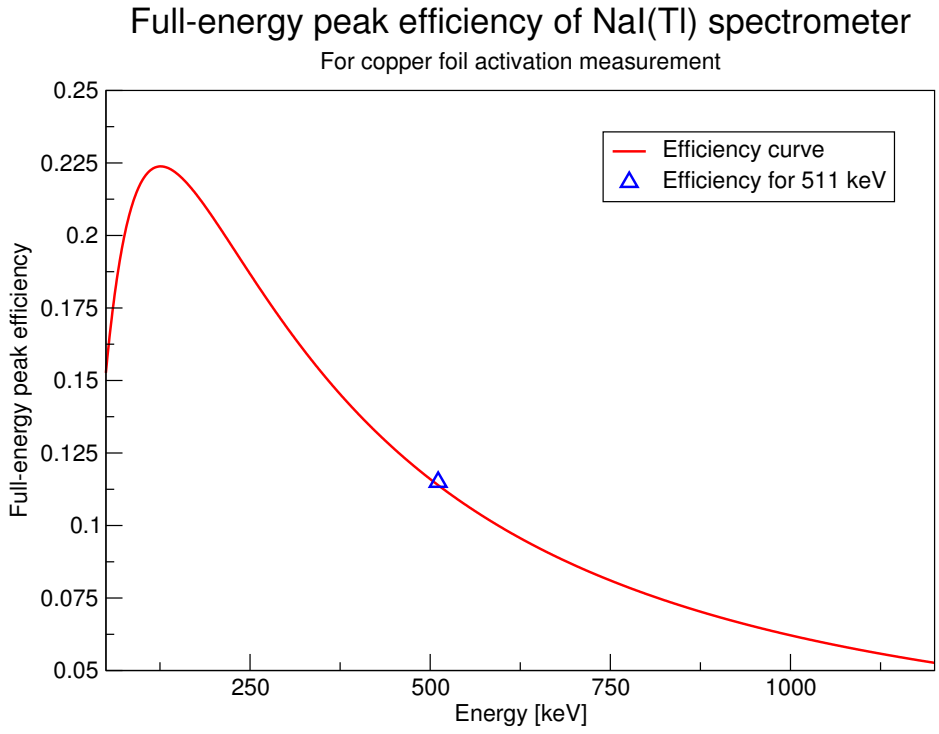

Figure 5.5: Full-energy peak efficiency of NaI(Tl) spectrometer for copper foil activation measurement.

The gamma spectrum of the activated copper foil is shown in Fig. 5.6. We can notice the significant peak resulting from the positrons released during the decay of ^{62}Cu and annihilated in surrounding lucite material.

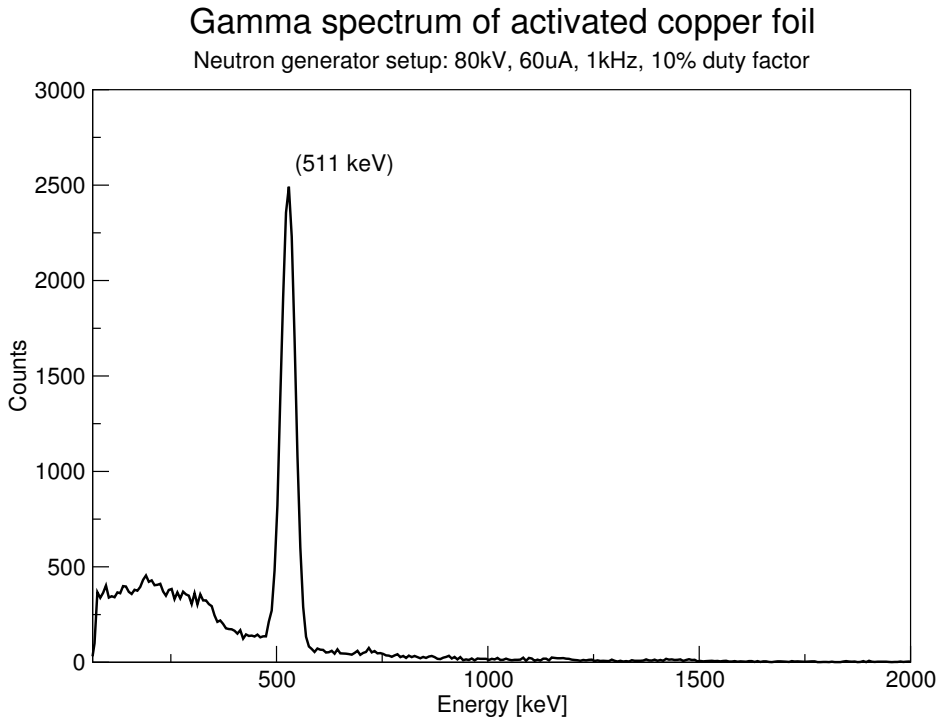

Figure 5.6: Gamma spectrum of a copper foil activated with 14 MeV neutrons showing significant annihilation peak.

5.4 Neutron Flux Calculation

As mentioned before the neutron flux of the generator depends on the setup, especially the setting of accelerator voltage and beam current but the flux depends also on the position of the foil (distance and angle) where we perform the measurement. The manufacturer states the neutron yield is approximately 10^8 neutrons per second (for 80 kV, 60μA, 10% duty factor, 1kHz pulse frequency) with the uncertainty estimated at 25%.

We performed the copper foil activation experiment under different conditions such as change of the accelerator voltage and the angle between the copper foil and the accelerator tube to observe dependence of the flux on changes of these conditions.

In order to determine the neutron flux some influences need to be resolved. The energy of the outcoming neutrons during T(d,n)^{4}He depends slightly on the angle at which the neutron escapes with respect to the direction of motion the accelerated deuterium ion (see Fig. 5.2). Since the energy can change during the different experimental setup (copper foil position), it means the absorption cross section for ^{63}Cu(n,2n)^{62}Cu reaction that is energy dependent (Section 2.3) changes as well at different angles of the copper foil position. The kinetic energy of the neutron can be derived from the conservation of momentum and

energy applied to Eq. 2.16 as following (see the complete derivation in Appendix B)

$$T_{n'} = \left(\frac{\sqrt{\frac{m_n \cdot m_d}{m_\alpha^2} \cdot T_d} \cdot cos\ \vartheta + \sqrt{\frac{m_n \cdot m_d}{m_\alpha^2} \cdot T_d \cdot cos^2\vartheta + \left(1 + \frac{m_n}{m_\alpha}\right) \cdot \left(\left(1 - \frac{m_d}{m_\alpha}\right) \cdot T_d + Q\right)}}{1 + \frac{m_n}{m_\alpha}} \right)^2 \tag{5.1}$$

where

- $T_{n'}$ is kinetic energy of neutron in MeV,
- T_d represents kinetic energy of deuterium ion in MeV,
- ϑ is the angle between the direction of motion of neutron and deuterium ion,
- Q is the energy of the reaction T(d,n)^{4}He,
- m_n is the mass of neutron in MeV,
- m_α refers to the mass of α particle in MeV and
- m_d is the mass of deuterium ion.

The kinetic energy of the fast neutrons was calculated for angles from 0° to 180° for 80 keV deuterium ions which we used for neutron flux measurement. The graph of the dependence between the angle and the energy is shown in Figure 5.7. The highest energy belongs to the neutrons deflecting at 0° and the lowest to those which escape at an angle of 180°. We performed our measurement for the angle 130° which belongs to the neutron energy of 13.70 MeV. We neglected deuterium ion energetic losses in the tritium target material because T(d,n)^{4}He cross section rapidly drops with the deuterium ion kinetic energy. However, more precise analysis of this effect will be envisaged in future if we obtain precise target configuration from the manufacturer.

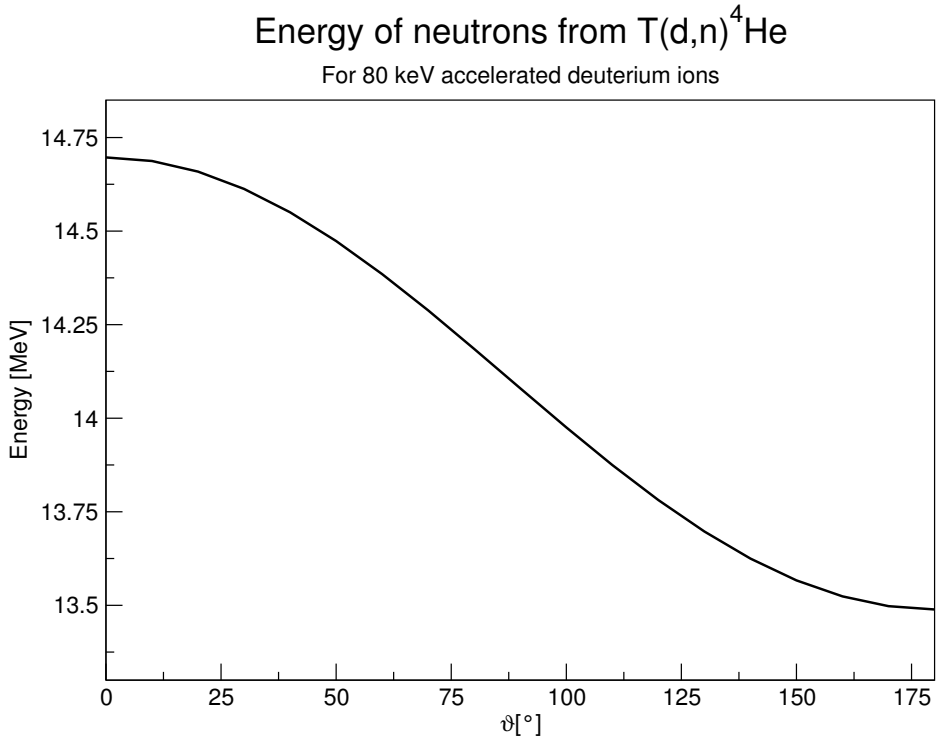

Figure 5.7: Energy of neutrons from T(d,n)^{4}He reaction depending on the neutron angle for 80 keV deuterium ions.

The kinetic energies of neutrons were further calculated for different acceleration voltage setups of neutron generator showing slightly diverse behaviour (see graph in Fig. 5.8). The calculated values of kinetic energies for different angles and acceleration voltages are stated in Appendinx C.

Now we can determine the cross section for ^{63}Cu(n,2n)^{62}Cu reaction for kinetic energy of neutrons $T = 13.70$ MeV. From EXFOR database [20] we overtook three different sets of cross section data (stated in Appendinx D) which were measured for the neutron kinetic energies from 13 MeV to 15 MeV. Data are displayed in Figure 5.9 with uncertainties. Ikeda data set (1994) was not used beacuse there is a significant deviation in cross sections from Mannhart (2007) and Sakane (2001). The remaining data sets were evaluated using linear regression in order to choose the best fitting data set for cross section calculation. Pearson correlation coefficient R_{corr} for both sets that is a measure of strength and direction of the linear relationship between the energy and the cross section [36], was determined using Grace plotting tool [37] (Table 5.4).

Data set	R_{corr}
Mannhart (2007)	0.990503
Sakane (2001)	0.976282

Table 5.4: Pearson correlation coefficients for cross section data sets.

Data set for which R_{corr} approaches closer to 1 is assumed to be a better fit. Thus for cross section calculation Mannhart cross section data set (2007) is selected. The linear regression

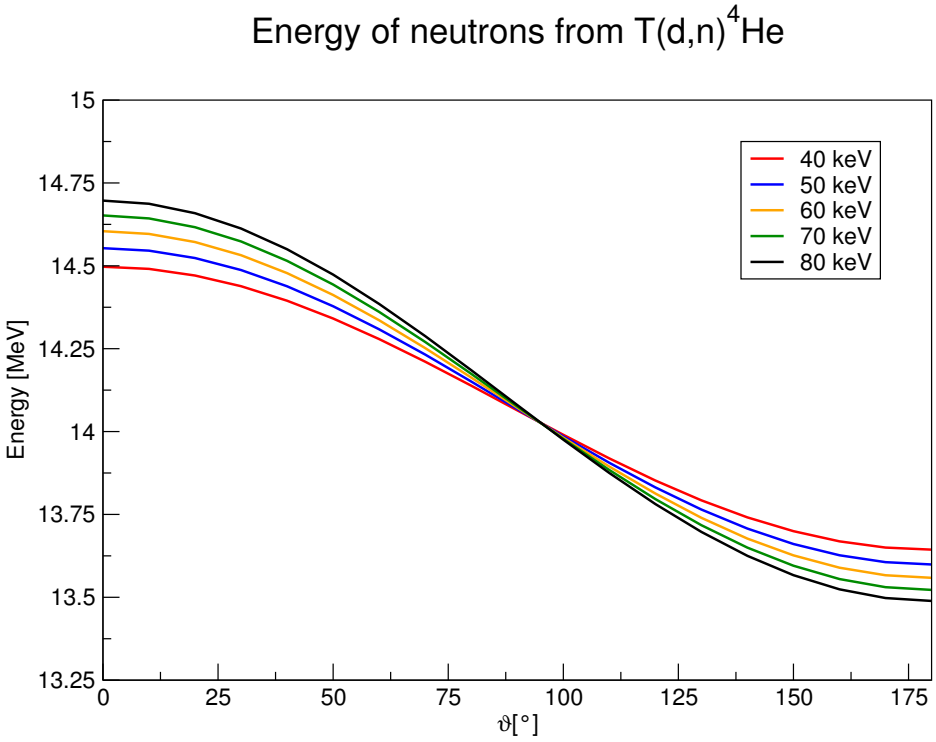

Figure 5.8: Energy of neutrons from T(d,n)^{4}He reaction depending on the neutron angle for various acceleration voltages of deuterium ions.

function for Mannhart (2007) is the following one

$$\sigma\ (\text{mb}) = -2102.90 + 182.59 \cdot E\ (\text{MeV}). \tag{5.2}$$

Using Eq. 5.2 we can easily determine the cross section for neutron energy at 130°:

$$\sigma\ (\text{mb}) = -2102.90 + 182.59 \cdot 13.70 = (400 \pm 15)\ \text{mb}. \tag{5.3}$$

So far we have determined all the values we needed to calculate the neutron flux for a given experimental setup (80 kV, 60 μA, 1 kHz, 10% DF, 130° and 17.2 cm) and the neutron yield for a given distance from the acceleration tube.

The neutron flux for the mentioned setup is calculated according to the Eq. 3.6

$$\varphi = (29\ 200 \pm 973)\ \text{cm}^{-2}\text{s}^{-1}.$$

This value expresses how many neutrons pass per unit area per second at the location of copper foil measurement. To obtain an approximate value of a neutron yield we multiply φ with the area of a sphere with the radius $r = 17.2$ cm which is the distance between the location of the copper foil and the target. The final approximate neutron yield for the given setup is evaluated using Eq. 3.7:

$$\varphi_0 = (1.082 \pm 0.037) \cdot 10^8\ \text{n/s}.$$

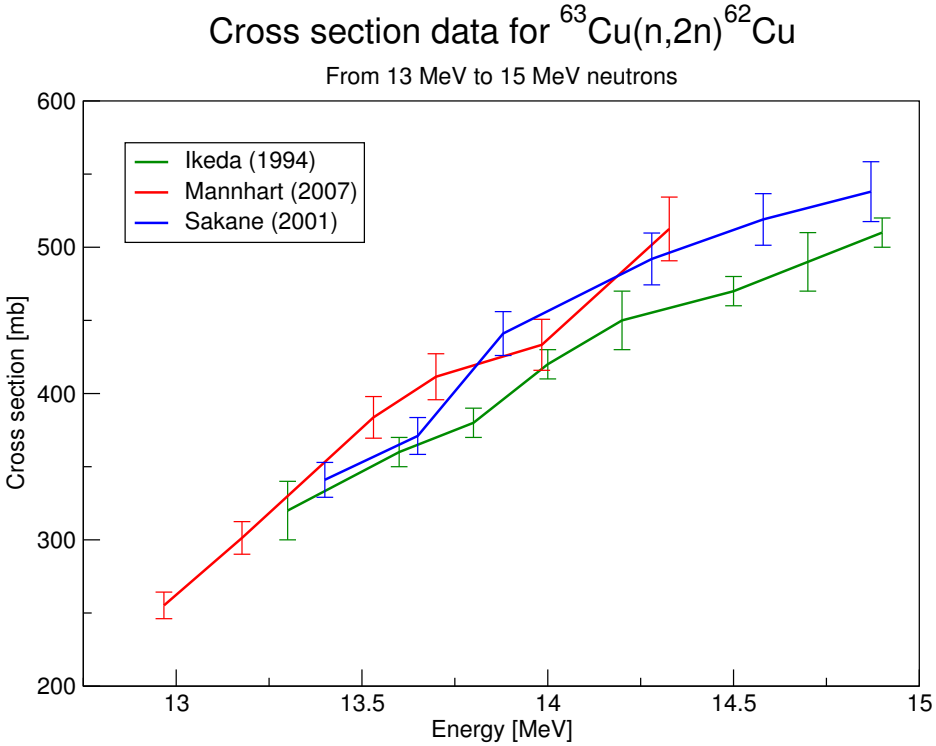

Figure 5.9: Cross section data for ^{63}Cu(n,2n)^{62}Cu reaction for neutrons from 13 MeV to 15 MeV.

Although the neutron yield tends to decrease with the lifetime of the accelerator tube, the value is very resembling with the value provided by the manufacturer. The reason for this may be that the neutron yield uncertainty provided by the manufacturer is very high (25%). We shall consider the manufacturer's neutron yield determination only as a rough estimation. The value of the neutron yield we determined is more precise with the uncertainty 3.34%.

The neutron flux dependence was further evaluated for different acceleration voltages. We performed copper foil activation experiment for the same experimental setup except we changed only the value of the acceleration voltage. We set the voltage on 80, 70, 60 and 40 kV respectively. The results are summarized in Table 5.10 and the dependence of the neutron yield on the acceleration voltage is shown in Fig. 5.10.

U (kV)	φ (cm^{-2}s^{-1})	φ_0 (n/s)
80	29200 ± 973	(1.082 ± 0.037)·10^8
70	18000 ± 638	(0.675 ± 0.024)·10^8
60	10000 ± 387	(0.380 ± 0.015)·10^8
40	1400 ± 208	(0.052 ± 0.008)·10^8

Table 5.5: Neutron flux and yield calculated for different acceleration voltage setups.

From Fig. 5.10 it is obvious that the neutron yield increases if the acceleration voltage increases. It shows quadratic dependence and the quadratic regression function

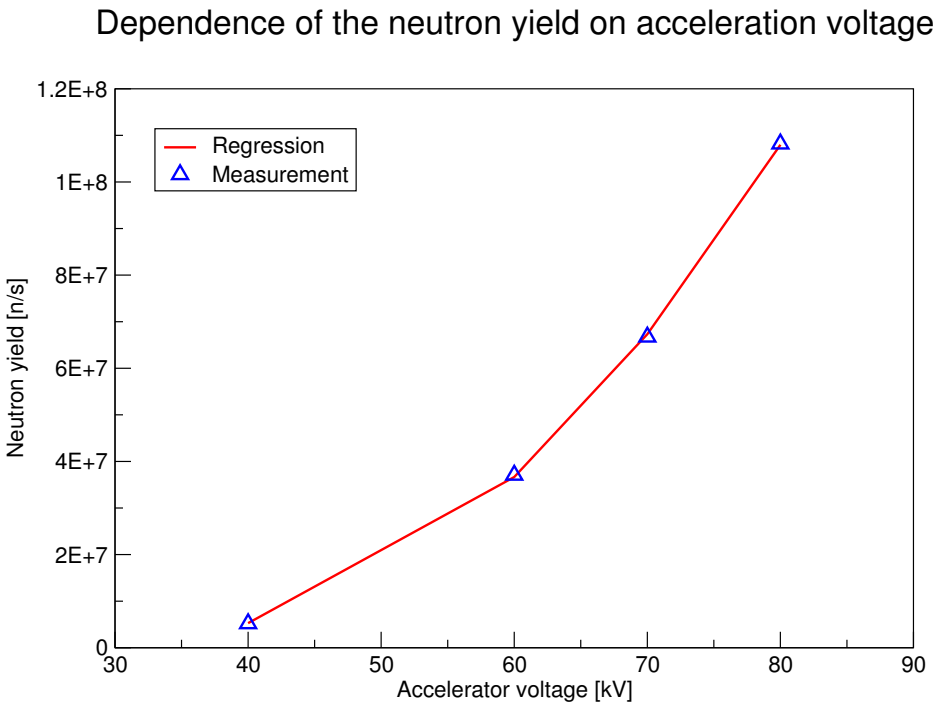

Figure 5.10: The dependence of the neutron yield on the acceleration voltage.

$$\varphi_0\ (\mathrm{n/s}) = 6.24 \cdot 10^7 - 3.43 \cdot 10^6 \cdot U\ (\mathrm{kV}) + 4.99 \cdot 10^4 \cdot U^2\ (\mathrm{kV})$$

allows us to estimate the neutron yield for acceleration voltages between 40 kV and 80 kV.

Chapter 6

Neutron Activation Analysis of Short-lived Radionuclides

In Section 3.1 two different approaches of how to measure gamma spectra of activated samples were introduced as prompt (PGNAA) and delayed gamma neutron activation analysis (DGNAA). To perform PGNAA gamma detector must be placed in the centre of irradiation next to neutron source and irradiated sample. This method is usually performed in the field when samples are are not possible to be collected and processed in a laboratory or elements being investigated are not possible to be measured using DGNAA. If a certain element can be measured by DGNAA, PGNAA is not suggested. During neutron activation radioactive nuclei are created and these have various half-lifes ranging from seconds to years. Concerning short half-lifes, about few seconds short, the detection of delayed gamma-rays must be conveniently quick. Otherwise PGNAA must be chosen. Table 6.1 shows some important elements and reactions during which short-lived radionuclides are produced.

Isotope	Reaction	$T_{1/2}$ (s)	E_γ (keV)	σ (mb)	P $_\gamma$ (%)
Boron	^{11}B(n,p)^{11}Be	13.8	2125	4.2	100
Oxygen	^{16}O(n,p)^{16}N	7.13	6129	35	67
Fluorine	^{19}F(n,p)^{19}O	26.91	197	19	95.9
Sodium	^{23}Na(n,α)^{20}F	11	1633	150	100
Sulfur	^{34}S(n,p)^{34}P	12.4	2127	74	15
Titanium	^{46}Ti(n,p)^{46m}Sc	18.7	142	48	62
Germanium	^{76}Ge(n,2n)^{75m}Ge	48.9	140	967	39
Selen	^{78}Se(n,2n)^{77m}Se	17.4	162	800	53
Yttrium	^{89}Y(n,n')^{89m}Y	16.1	909	438	99
Molybdenum	^{92}Mo(n,2n)^{91m}Mo	65	653	14.5	48
Cerium	^{140}Ce(n,2n)^{139m}Ce	55	754	960	93
Gold	^{197}Au(n,n')^{197m}Au	7.73	279	280	71
Lead	^{204}Pb(n,2n)^{203m1}Pb	6.1	825	1200	71

Table 6.1: Isotopes forming short-lived radionuclides after irradiation with 14 MeV neutrons [38].

In our case we measured gamma spectra of samples containing elements producing short-

lived radionuclides after activation with 14 MeV neutrons. Samples were transported with the use of pneumatic transport system in the laboratory. The pneumatic transport system we prepared (Section 6.2) allows us to transport samples quickly in a proper container from neutron generator to gamma spectrometer and vise versa.

Following sections describe first the laboratory for Neutron Activation Analysis and Gamma Spectrometry in Ostrava, its instruments and possible areas of research. Then it focuses on the pneumatic transport system that is used when short-lived radionuclides are present in the sample. After that NAA procedure is described and some of the results from measuring selected elements are illustrated in the last part including determination of mass of short-lived radionuclides.

6.1 Laboratory for Neutron Activation Analysis and Gamma Spectrometry

The laboratory for neutron activation analysis (NAA) and gamma spectrometry (GS) at VŠB-TUO built in 2016 is located in the shallow underground next to the Planetarium of Johann Palisa in Ostrava. Besides the neutron activation analysis low-level gamma spectrometry [2] of environmental samples is envisaged in the laboratory. Therefore, low detection background and its precise measurement are crucial points to be addressed.

The laboratory consists of two main rooms (as seen in Fig. 6.1) located four meters below the ground level, and an entrance with a lift. One of the room (on the left in Fig. 6.1) works as an operation and detection room with one HPGe and one scintillation spectrometer, laboratory instruments and computer equipment. The second room (on the right in Fig.

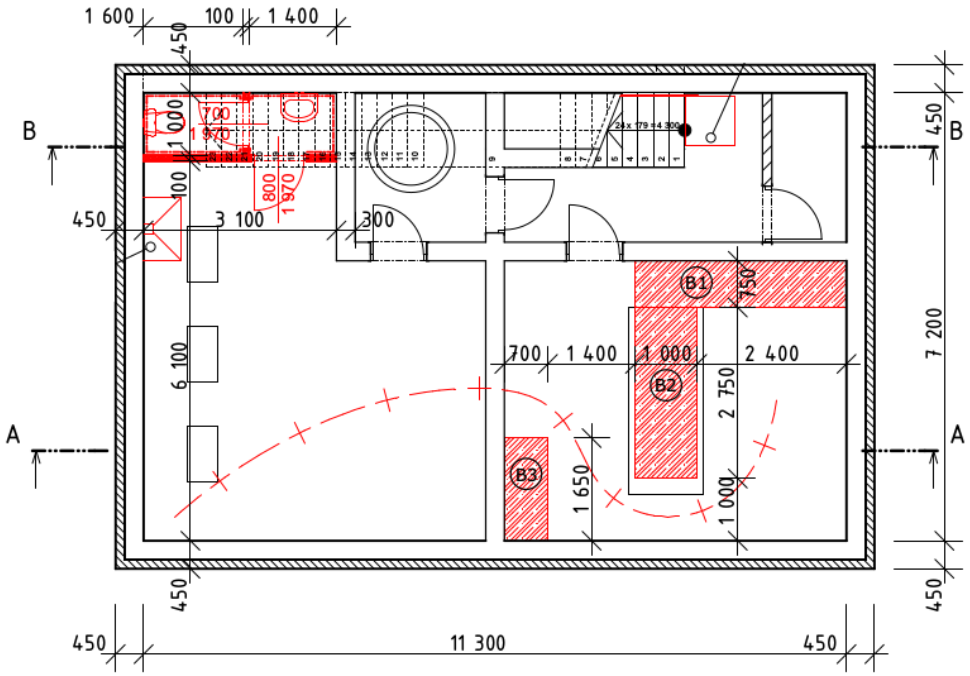

Figure 6.1: Top view of the Neutron activation analysis laboratory at VŠB-TUO (length in meters).

6.1) is equipped with one meter thick concrete shielding (marked by red color) to moderate the outcoming neutrons and shield γ radiation. The neutron generator is placed behind the shielding. The red dotted curved line going over both of the rooms represents the pneumatic transport system used for quick sample transport from the neutron generator to the spectrometer and vise versa.

The core instruments of the laboratory are the Thermo Fisher Scientific MP320 NG, Canberra NaI(Tl) scintillation spectrometer and Baltic Scientific Instruments well-type HPGe spectrometer GWD-3023 [34]. The compact MP320 NG [35] produces 14 MeV neutrons and was already mentioned in Section 5. The standard NaI(Tl) spectrometer is placed in 10 cm lead shielding with two inner 1 mm thick Cd and Cu liners. The 30 % relative efficiency well-type HPGe spectrometer GWD-3023 operates in an energy range of 20 keV – 10 MeV. The well dimensions are 16 mm in diameter and 50 mm in depth (see Fig. 6.2). Detector ultra-low background cryostat is made from ultra pure Al (5N5 AlSi 1%), OFE-OK electrolytic copper and its uranium and thorium content is less than 1 ppb. The detector is placed in 10 cm lead shielding with 8 mm radio pure copper liner. Activity of natural occurring radionuclides in the 2 cm inner chamber of the lead shield is less than 5 Bq/kg.

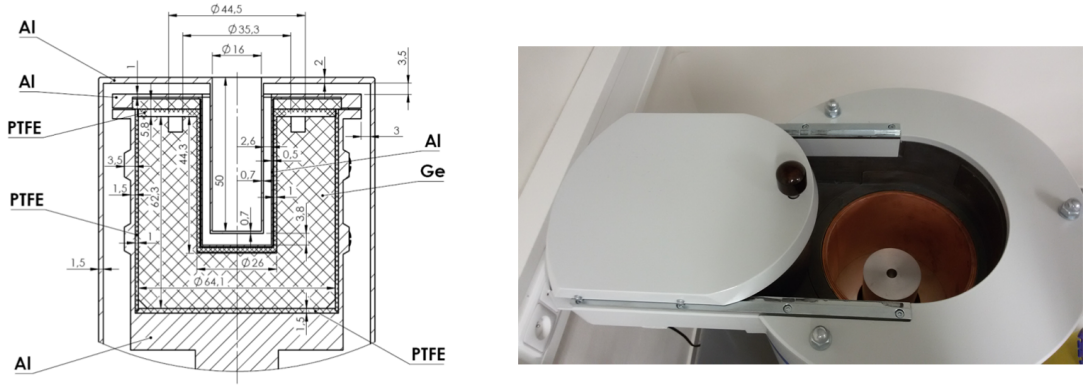

Figure 6.2: Design of the HPGe GWD-3023 spectrometer and end cup (left), the spectrometer with an opened shielding (right).

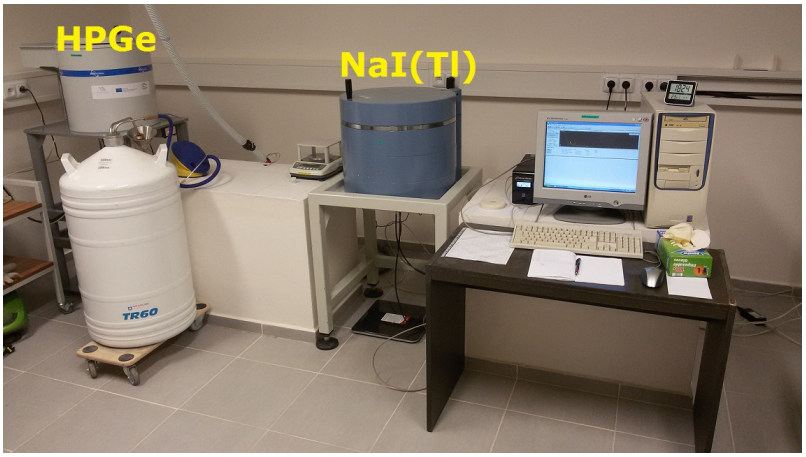

Figure 6.3: Part of the laboratory with well-type HPGe (left) and NaI(Tl) spectrometers (right).

6.2 Pneumatic Transport System

To transport samples from the neutron generator to the spectrometer and to prevent radiation dosage a pneumatic transport system was developed. In Fig. 6.1 there is a red dotted curved line representing the transport pipe used for quick transport of samples. A person operating the neutron generator does not need to pick up the activated sample by hand but can easily send it straight to the spectrometer. Also short-lived radionuclides created during 14 MeV activation decaying within few seconds or minutes may be detected. Figure 6.4 shows part of the operation room and the transport pipe as a part of the transport system.

Figure 6.4: Operation room showing part of the transport pipe used for transporting samples.

Each ending of the pipe is connected to the air pump that is operated manually and to the spectrometer or neutron generator as shown in a scheme in Fig. 6.5. There is also a detection system made from Arduino components [39] to detect the motion and the location of a sample. The detection is provided using infrared sensors that can detect the motion of a transporting sample container. In Fig. 6.6 the real implementation of the transport system is seen.

The sample can be transported in both directions as requested. The pump soaks up the air that pushes and transports the sample in the direction of the air pump within few seconds (approximately 4 seconds in average, it may be longer depending on the weight of the sample). Using the arduino detection system we are able to see if the sample was transported correctly and to measure the transportation time.

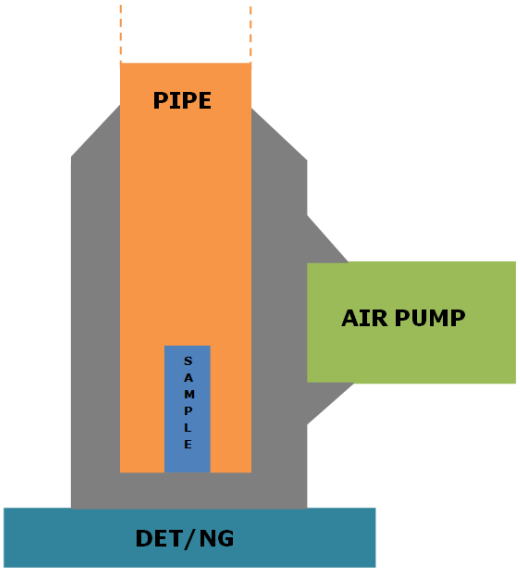

Figure 6.5: Scheme of the ending of the pipe connected either to the detector or the neutron generator.

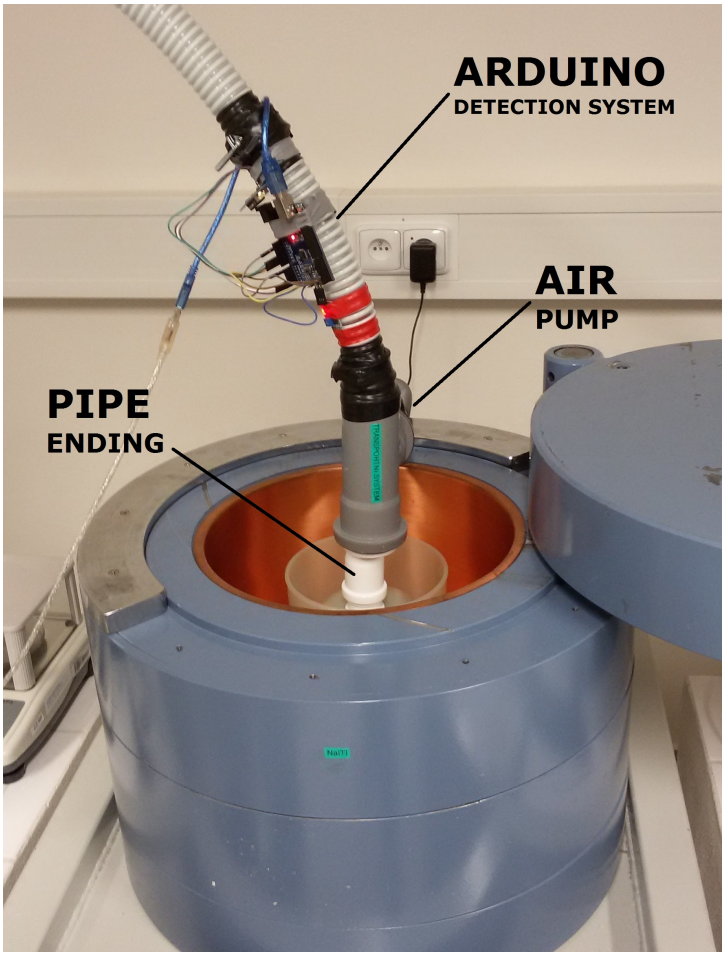

Figure 6.6: Transport system ending connected to the scintillation spectrometer.

6.3 NAA Measurement Procedure

In the Laboratory for Neutron activation analysis and Gamma spectrometry we perform DGNAA measurement in the following way:

At first sufficient amount of sample for analysis should be homogenized and placed into a proper sample container. It is important to know which elements are required to be measured so that a proper choice of neutron induced reactions and standards could be used. The presence of interfering components with investigated elements in the sample have to be taken into account.

If the requirements are fulfilled irradiation of the sample can begin. A typical irradiation time depends on the half-life of the investigated element. After irradiation the sample is transfered to gamma spectrometer where gamma-rays are counted. If possible, the transport of the sample should be performed through a pneumatic transport system directly into the spectrometer to avoid personal contamination. Irradiation time, transportation time from neutron source to gamma counter and measurement time in the counter must be noted for further calculations.

After measuring the gamma spectrum it is evaluated using gamma libraries or other nuclear database to identify isotopes in the sample. To be able to calculate concentrations in the sample using relative method, a prepared standard is irradiated and measured upon the same conditions as the sample. If absolute method is used, neutron flux for a given setup of the neutron source must be determined. Using measurement equations for NAA (3.1 and 3.2) it is possible to determine concentrations of investigated elements from the gamma peak area for a given energy. The efficiency of gamma energy detection varies with different energies and geometries thus efficiency curve of the used spectrometer must be obtained before calculations.

6.4 Mass Measurement of Short-lived Radionuclides

Neutron induced reactions characterized by high cross sections were selected to perform first NAA measurement of short-lived radionuclides in the Laboratory for NAA and GS. Some other isotopes were activated (see Table 6.1) but not properly detected bacause of low cross section for the particular reaction, low gamma emission probability or due to longer transportation time than the half-life of the formed radionuclide. The following isotopes showed significant sensitivity for 14 MeV neutron activation:

$$^{89}\mathrm{Y(n,n')}^{89m}\mathrm{Y} : \sigma_{nn'} = 438 \text{ mb},$$

$$^{140}\mathrm{Ce(n,2n)}^{139m}\mathrm{Ce} : \sigma_{n2n} = 960 \text{ mb}.$$

Two samples containing a given amount of these isotopes in the compounds Y_2O_3 and CeO_2 were irradiated using 14 MeV neutrons, after a certain time transported to the gamma spectrometer using the pneumatic transport system and then gamma spectrometry data were measured. Delayed gamma spectra of both activated samples are displayed in Fig. 6.8

and 6.7. Significant peaks at 754 keV and 909 keV indicates the presence of investigated isotopes. From natural background radiation the peaks from the decay of ^{40}K is recognized. The samples were irradiated with the neutron flux $\varphi = (29\ 200 \pm 973)\ \mathrm{cm}^{-2}\mathrm{s}^{-1}$. Gamma spectrometry data collected using NaI(Tl) spectrometer and pneumatic transport system are summarized in Table 6.2.

Compound	C	t_i (s)	t_d (s)	t_m (s)
CeO_2	776 ± 53	300	4	140
Y_2O_3	237 ± 33	180	3	96

Table 6.2: Gamma spectrometry data measured for CeO_2 and Y_2O_3 after their 14 MeV activation.

Using Eq. 3.1 we are able to determine the mass of ^{140}Ce and ^{89}Y isotopes in the samples from the measured number of counts C. The knowledge of the isotope abundance and the molar mass [40] are requested for the calculation (see Table 6.3). The current value of Avogadro constant N_{av} equals $6.02214 \cdot 10^{23}\ \mathrm{mol}^{-1}$ [41].

Isotope	θ (%)	M_A (g/mol)
^{140}Ce	88.4	140.16
^{89}Y	100	88.91

Table 6.3: Abundance θ and molar mass M_A of ^{140}Ce and ^{89}Y isotopes.

Efficiency curve is requested for the purpose of determining the efficiency for 754 keV and 909 kev (measured gamma-ray energy). Using SpectraLineGP, the model of NaI(Tl) spectrometer (Figure 4.6) and the dimensions and geometry of activated content and sample container (Figure 6.9) we simulated the efficiency curves in order to use them for mass calculation of activated samples. The efficiency curves for this case are shown in Fig. 6.10. Efficiency values of requested gamma energy are labeled in the graph and stated in Table 6.4.

The sample container is approximately 0.4 cm distant from the spectrometer surface due to the wall thickness of the ending of pneumatic transport system. This results in lower efficiency of the spectrometer.

Isotope	E_γ (keV)	Efficiency
^{140}Ce	754	0.0669 ± 0.0028
^{89}Y	909	0.0586 ± 0.0026

Table 6.4: Full-energy peak efficiency of NaI(Tl) spectrometer for 754 keV and 909 keV.

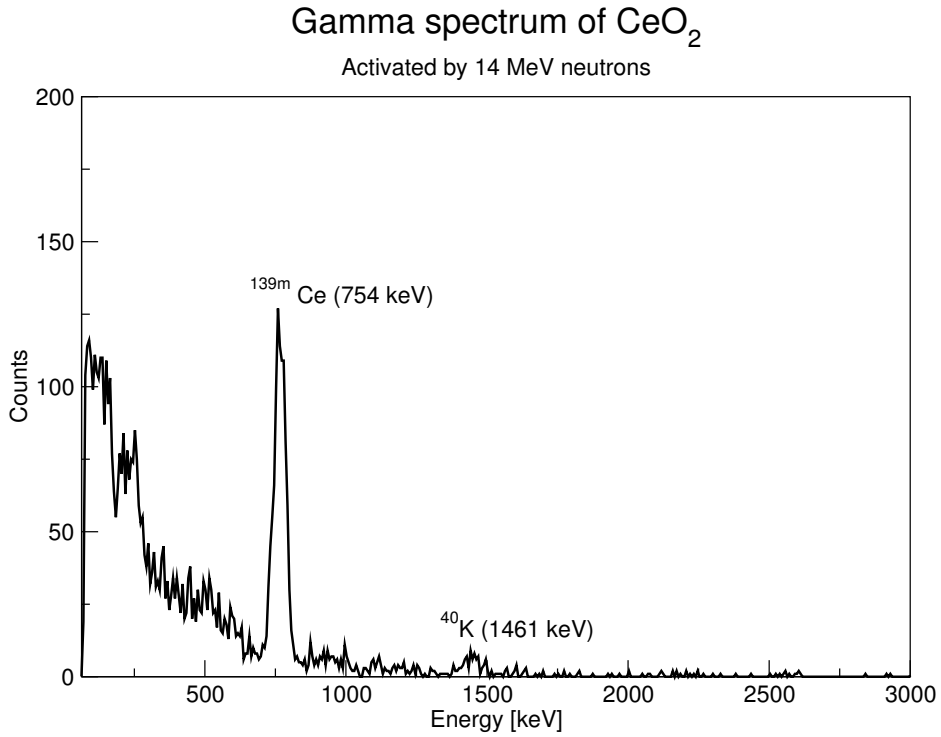

Figure 6.7: Gamma spectrum of CeO_2 activated by 14 MeV neutrons and measured on NaI(Tl) scintillation spectrometer.

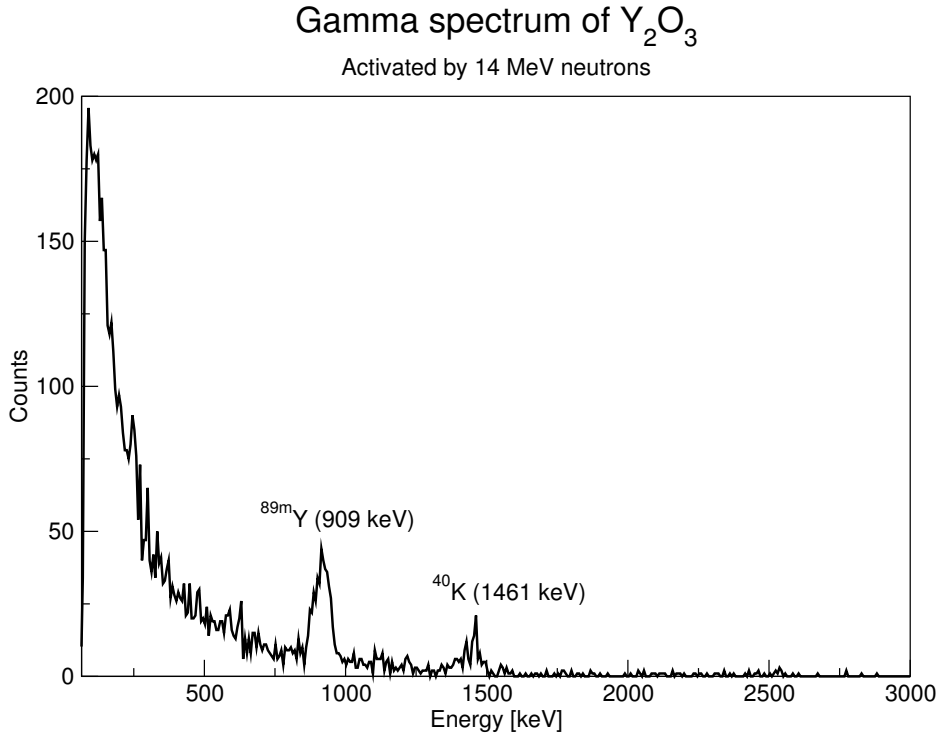

Figure 6.8: Gamma spectrum of Y_2O_3 activated by 14 MeV neutrons and measured on NaI(Tl) scintillation spectrometer.

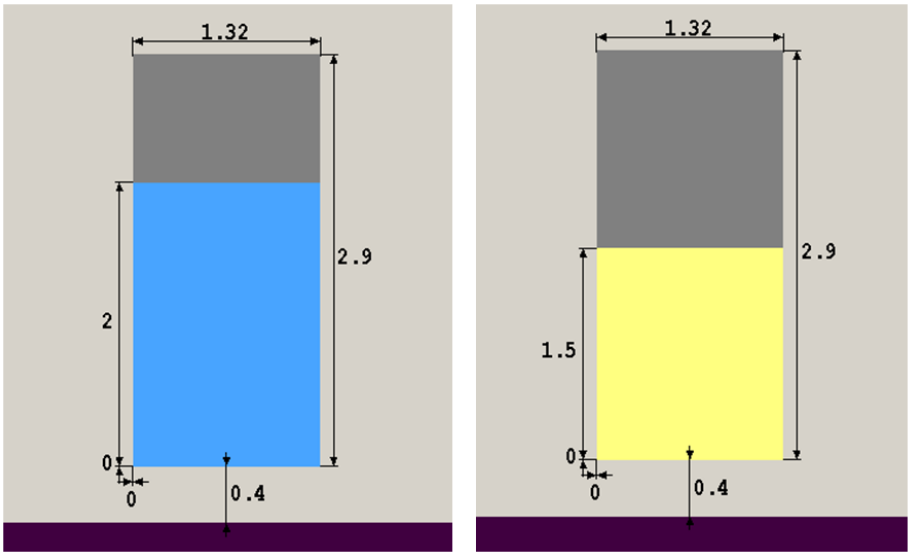

Figure 6.9: Model of the sample containers for simulation of efficiency for NAA measurement of short-lived radionuclides (in cm). Blue color represents the activated content of Y_2O_3 and yellow color represents the content of CeO_2 sample. Grey color refers to the empty space in the container.

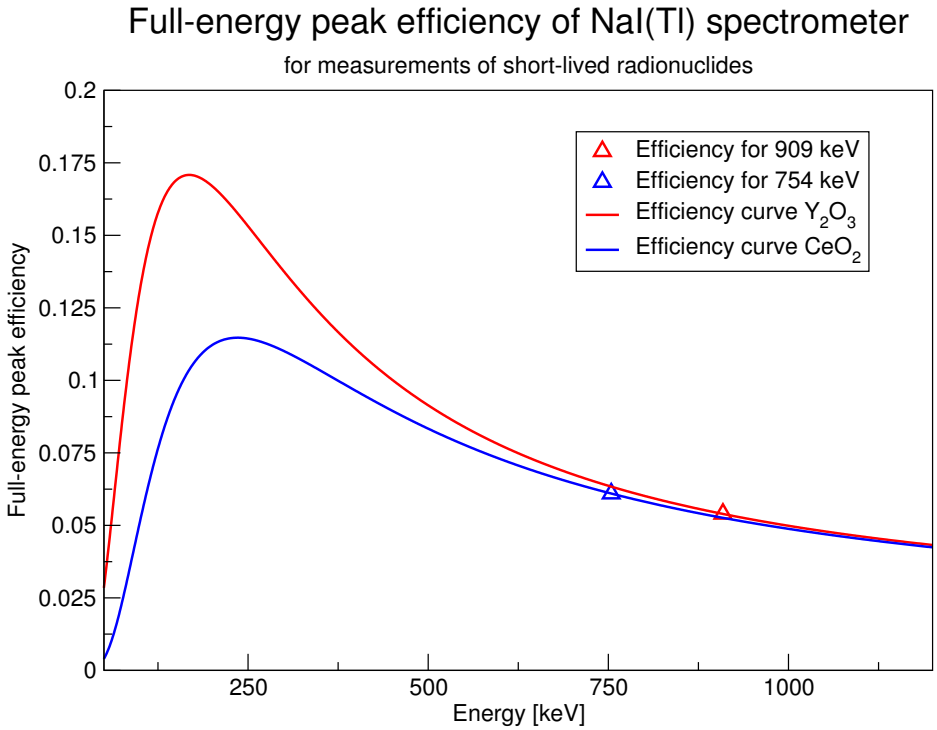

Figure 6.10: Full-energy peak efficiency of NaI(Tl) spectrometer for measurement of short-lived radionuclides.

By determining the efficiency of the spectrometer for the given energy we are able to investigate the total mass of the isotope in the sample content by simply using the Eq. 3.1. In Table 6.5 the measured masses of ^{140}Ce and ^{89}Y isotopes are shown. To evalute the method accuracy the mass of the isotopes can be calculated from the knowledge of the mass of compound and the molar masses using an amount of substance ($n = m/M_A$) [42]. The mass of CeO_2 sample is 2.00 g and the mass of Y_2O_3 sample is 2.80 g, weighed on analytical scales with an uncertainty of 0.03 g. Molar masses and isotope abundances of ^{140}Ce, ^{89}Y are given in Table 6.3 and the molar mass of ^{16}O is 15.99 g/mol [43]. The masses calculated by this approach are summarized in Table 6.5 in the third column as m_D.

Isotope	m_A (g)	m_D (g)
^{140}Ce	1.92 ± 0.17	1.45 ± 0.025
^{89}Y	2.35 ± 0.36	2.21 ± 0.012

Table 6.5: Measured ^{140}Ce and ^{89}Y masses in the samples.

The mass m_D is more accurate as it is directly measured. However, it is noticable the results obtained by NAA are very resembling with the real mass values. We can assume the presented approach may be used for detection and mass measurement of short-lived radionuclides. However, cross section data given in Table 6.1 used in our calculations may be the reason for the mass deviation at ^{140}Ce isotope. It implies that a more accurate analysis of dependence of the cross sections for short-lived radionuclides on neutron energy should be conducted, as in Section 5.4 for ^{63}Cu.

Conclusion

In this thesis we have presented an application of Texas convention technique in order to determine the neutron flux and neutron yield of Thermo Fisher Scientific MP 320 Neutron Generator that is a core instrument in the Laboratory for Neutron Activation Analysis and Gamma Spectrometry at VŠB-TU in Ostrava. We collected our experimental data using NaI(Tl) scintillation spectrometer for which efficiency calibration was established by means of computer simulation in SpectraLineGP software and the resulting efficiency calibration was verified by four point gamma sources with known activities. A significant part of the work includes the construction of pneumatic transport system developed for transportation of samples from the neutron generator to gamma spectrometer in few seconds allowing us to detect and analyze short-lived radionuclides formed during 14 MeV neutron activation. In the final part we presented neutron activation analysis of selected short-lived radionuclides using the pneumatic transport system and the results from neutron flux determination that led into obtaining the masses of isotopes which formed the selected short-lived radionuclides.

We conducted in-depth exploration of dependence of the neutron flux and yield on different acceleration voltages and calculated the values of the neutron flux and yield for 40 keV, 60 keV, 70 keV and 80 keV deuterium ions. For 80 keV deuterium ions we obtained the neutron yield $\varphi_0 = (1.082 \pm 0.037) \cdot 10^8$ n/s. For the same NG setup the manufacturer provides an estimated value of neutron yield $\varphi_0 = (1.00 \pm 0.25) \cdot 10^8$ n/s showing significantly high uncertainty of 25%. Our measurement demonstrates far more accurate values (uncertainty 3.34%) and so the results have been used in NAA calculations carrying lower uncertainties to the final analysis of isotope masses. We prepared samples containing CeO_2 and Y_2O_3 compounds in order to investigate the mass of ^{140}Ce and ^{89}Y isotopes using neutron activation analysis and compared the method accuracy with the results from direct measurement of the isotope masses using analytical scales. Both the isotopes form short-lived radionuclides after 14 MeV activation so the pneumatic transport system was used to detect the gamma energies on the scintillation counter. Based on the determined value of the neutron flux and collected gamma spectrometry data the mass of ^{140}Ce was obtained as $m_A(\mathrm{Ce}) = (1.92 \pm 0.17)$ g and the mass of ^{89}Y was equal $m_A(\mathrm{Y}) = (2.35 \pm 0.36)$ g. In comparison with the directly measured masses of the isotopes $m_D(\mathrm{Ce}) = (1.45 \pm 0.025)$ g and $m_D(\mathrm{Y}) = (2.21 \pm 0.012)$ g we conclude that the results are satisfying for first test measurement of short-lived radionuclides in the Laboratory for NAA and GS in Ostrava by this approach.

The presented method can be used for investigation of other major or minor isotopes, for example ^{23}Na, ^{76}Ge, ^{197}Au and ^{204}Pb showing higher cross sections. We attempted to analyze ^{16}O or ^{34}S using 14 MeV neutron activation analysis but we could not achieve accurate results due to low cross sections for the reactions, very short half-lifes and released high energetic gamma-rays were related with very low detector efficiency. The possible approach is to use prompt gamma neutron activation analysis in order to detect these isotopes.

The major contributions of this work are that we determined the neutron flux of the neutron generator for selected experimental setups, we were able to construct the pneumatic transport system for measurement of short-lived radionuclides and apply the absolute method to measure masses of selected isotopes by neutron activation analysis. We intend to futher examine the neutron flux of MP 320 NG with regard to the angle of irradiation, changing foil thicknesses to determine very low neutron fluxes and to use different foil materials, such as aluminium, iron and indium. The detailed examination of neutron flux brings more accurate results in NAA. We also plan to connect the transport system with HPGe spectrometer GWD-3023 showing greater efficiency and energy resolution to provide more accurate measurements.

Bibliography

[1] PAUL A. TIPLER. Physics. 2nd ed. [illustrated by Felix Cooper and John Kramer]. New York, N.Y: Worth Publishers, 1982. ISBN 08-790-1135-1.

[2] GILMORE, Gordon. Practical gamma-ray spectrometry. 2nd ed. Hoboken, NJ: Wiley, c2008. ISBN 978-047-0861-967.

[3] WALKER, Jearl and David HALLIDAY. Fundamentals of physics. 9th ed., extended. Hoboken, NJ: Wiley, c2011. ISBN 978-047-0564-738.

[4] Nucleonica [online]. Germany: Institute for Transuranium Elements, 2017 [cit. 2017-03-22]. Available at: http://www.nucleonica.com/

[5] HALLIDAY, David, Robert RESNICK and Jearl WALKER. Fyzika: vysokoškolská učebnice obecné fyziky. Brno: VUTIUM, 2000. ISBN 80-214-1868-0.

[6] NAVRÁTIL, Leoš and Jozef ROSINA. Medicínská biofyzika. Praha: Grada, 2005. ISBN 80-247-1152-4.

[7] WILLIAM R. LEO. Techniques for nuclear and particle physics experiments: a how-to approach. Corr. 2nd print. Berlin: Springer-Verlag, 1992. ISBN 35-401-7386-2.

[8] ATWOOD, David A. Radionuclides in the environment. New York: Wiley, c2010. EIC books. ISBN 04-707-1434-4.

[9] COOMBER, D. I. Radiochemical methods in analysis. New York: Plenum Press, 1975. ISBN 03-063-0738-3.

[10] The Lund/LBNL Nuclear Data Search: Version 2.0, February 1999 [online]. Berkeley, USA, Lund University, Sweden: LBNL/Department of Physics, 1999 [cit. 2017-04-19]. Available at: http://nucleardata.nuclear.lu.se/toi/index.asp

[11] L'ANNUNZIATA, Michael F (ed.). Handbook of radioactivity analysis. 3rd ed. Oxford: Elsevier, 2012, xxxvii, 1379 s. ISBN 978-0-12-384873-4.

[12] ŠTOLL, Ivan. Dějiny fyziky. Praha: Prometheus, 2009. ISBN 978-80-7196-375-2.

[13] WILLIS, B. T. M. and C. J. CARLILE. Experimental neutron scattering. New York: Oxford University Press, 2009. ISBN 01-985-1970-2.

[14] OLIVE, K.A. Review of Particle Physics. Chinese Physics C. 2016, 40(10), 100001-. DOI: 10.1088/1674-1137/40/10/100001. ISSN 1674-1137, http://stacks.iop.org/1674-1137/40/i=10/a=100001?key=crossref.5ca5f9c166adc59f41e03a802b715c19

[15] VLASOV, Nikolaj Aleksandrovič. Neutrony. Praha: Československá akademie věd, 1958.

[16] PODGORŠAK, E. Radiation physics for medical physicists. 2nd, enlarged ed. Berlin: Springer, 2010, xxxiii, 745 s. Biological and medical physics, biomedical engineering. ISBN 978-364-2008-740.

[17] BACON, G. E. Neutron diffraction. 3d ed. Oxford [Eng.]: Clarendon Press, 1975. ISBN 978-019-8513-537.

[18] Overview of Neutron Activation Analysis. Archaeometry Laboratory: University of Missouri Research Reactor[online]. Missouri, Columbia, 2015, http://archaeometry.missouri.edu/naa_overview.html

[19] VIERERBL, L., M. VINŠ, Z. LAHODOVÁ, A. FUKSA, J. KUČERA, M. KOLEŠKA and A. VOLJANSKIJ. Mercury mass measurement in fluorescent lamps via neutron activation analysis. Radiation Physics and Chemistry. 2015, 116, 56-59. DOI: 10.1016/j.radphyschem.2015.03.041. ISSN 0969806x. Available at: http://linkinghub.elsevier.com/retrieve/pii/S0969806X15001292

[20] National Nuclear Data Center [online]. Brookhaven National Laboratory [cit. 2017-04-19]. Available at: http://www.nndc.bnl.gov/

[21] INTERNATIONAL ATOMIC ENERGY AGENCY. Neutron generators for analytical purposes. Vienna: International Atomic Energy Agency, 2012. ISBN 978-920-1251-107.

[22] MEDHAT, M.E. Fast neutron activation analysis by means of low voltage neutron generator. Results in Physics. 2016, 6, 860-862. DOI: 10.1016/j.rinp.2016.02.004. ISSN 22113797. Available at: http://linkinghub.elsevier.com/retrieve/pii/S2211379716000243

[23] MARCHESE, N., A. CANNULI, M.T. CACCAMO and C. PACE. New generation non-stationary portable neutron generators for biophysical applications of Neutron Activation Analysis. Biochimica et Biophysica Acta (BBA) - General Subjects. 2017, 1861(1), 3661-3670. DOI: 10.1016/j.bbagen.2016.05.023. ISSN 03044165. Available at: http://linkinghub.elsevier.com/retrieve/pii/S0304416516301659

[24] SHULYAKOVA, Olga, Petr AVTONOMOV and Valeria KORNIENKO. New Developments of Neutron Activation Analysis Applications. Procedia - Social and Behavioral Sciences. 2015, 195, 2717-2725. DOI: 10.1016/j.sbspro.2015.06.380. ISSN 18770428. Available at: http://linkinghub.elsevier.com/retrieve/pii/S1877042815038598

[25] PEETERMANS, Steven. Neutron Activation Analysis [online]. Rez, The Czech republic, 2009 [cit. 2016-05-17]. Available at: https://ojs.ujf.cas.cz/ wagner/transmutace/studentpraxe/stevenreferat.pdf

[26] BARZILOV, A., B. KESSLER and P.C. WOMBLE. Analysis of 14-MeV neutron induced gamma-ray spectra using multiwavelets. Radiation Measurements. 2015, 79, 43-49. DOI: 10.1016/j.radmeas.2015.06.007. ISSN 13504487. Available at: http://linkinghub.elsevier.com/retrieve/pii/S135044871530038X

[27] ALEXA, Petr and Radim UHLÁŘ. The first test of the new neutron generator at the VŠB - Technical university of Ostrava. GeoScience Engineering. 2013, (59), 1-5. ISSN 1802-5420.

[28] BARZILOV, Alexander and Ivan NOVIKOV. Material Classification by Analysis of Prompt Photon Spectra Induced by 14-Mev Neutrons. Physics Procedia. 2015, 66(2), 396-402. DOI: 10.1016/j.phpro.2015.05.049. ISSN 18753892. Available at: http://linkinghub.elsevier.com/retrieve/pii/S1875389215002023

[29] MOLNAR, Gabor L. Handbook of prompt gamma activation analysis with neutron beams. Boston: Kluwer Academic Publishers, c2004. ISBN 978-0-387-23359-8.

[30] DORON, Oded, Lucian WIELOPOLSKI, Sudeep MITRA a Steven BIEGALSKI. MCNP benchmarking of an inelastic neutron scattering system for soil carbon analysis. Nuclear Instruments and Methods in Physics Research Section A: Accelerators, Spectrometers, Detectors and Associated Equipment. 2014, 735, 431-436. DOI: 10.1016/j.nima.2013.09.049. ISSN 01689002. http://linkinghub.elsevier.com/retrieve/pii/S0168900213012837

[31] STRELLIS, Dan and Tsahi GOZANI. Classifying threats with a 14-MeV neutron interrogation system. Applied Radiation and Isotopes. 2005, 63(5-6), 799-803. DOI: 10.1016/j.apradiso.2005.05.037. ISSN 09698043. Available at: http://linkinghub.elsevier.com/retrieve/pii/S0969804305001697

[32] KORNIENKO, Valeria and Petr AVTONOMOV. Application of Neutron Activation Analysis for Heavy Oil Production Control. Procedia - Social and Behavioral Sciences. 2015, 195, 2451-2456. DOI: 10.1016/j.sbspro.2015.06.277. ISSN 18770428. Available at: http://linkinghub.elsevier.com/retrieve/pii/S1877042815037568

[33] Canberra Industries, Inc., Scintillation detectors, available at: http://www.canberra.com/products/ detectors/scintillation-detectors.asp

[34] Gamma-ray spectrometer based on well-type HPGe detector GWD-3023, Passport and operating manual, corporation: Baltic Scientific Instruments, Riga, 2016

[35] Thermo Scientific MP 320 Lightweight, Portable Neutron Generator, corporation: Thermo Fisher Scientific, Colorado Springs, 2007

[36] MONTGOMERY, Douglas C., Elizabeth A. PECK and G. Geoffrey VINING. Introduction to linear regression analysis. 5th ed. Hoboken, NJ: Wiley, 2012. ISBN 978-0-470-54281-1.

[37] Grace [online]. [cit. 2017-04-30]. Available at: http://plasma-gate.weizmann.ac.il/Grace/

[38] AKSOY, A., F.Z. KHIARI and M. AL-HADDAD. Sensitivities of 14 MeV Neutron Activation Analysis Using a Drift-Tube Neutron Generator at KFUPM. ARABIAN JOURNAL FOR SCIENCE AND ENGINEERING. 2003, 28(1)

[39] Arduino [online]. 2017 [cit. 2017-04-30]. Available at: https://www.arduino.cc/

[40] Molar Mass Calculator [online]. [cit. 2017-04-08], http://www.webqc.org/mmcalc.php

[41] Fundamental Physics Constants [online]. [cit. 2017-05-07], http://physics.nist.gov/cgi-bin/cuu/Value?na|search_for=avogadro

[42] Amount of substance [online]. [cit. 2017-05-01], https://en.wikipedia.org/wiki/Amount_of_substance

[43] Periodic Table of Elements [online]. [cit. 2017-04-15], https://iupac.org/what-we-do/periodic-table-of-elements/

List of Figures

List of Tables

Acknowledgement

I would like to express my great gratitude to my supervisor Doc. Dr. RNDr. Petr Alexa for the useful comments, remarks and engagement through the whole learning process of this master thesis. Furthermore I would like to thank Dr. Radim Uhlář and Bc. Pavlína Haroková for a great help during the completion of the thesis and with the measurements in the laboratory.

Appendices

Appendix A

Gamma spectrum of ^{152}Eu used for verifying the accuracy of energy calibration of scintillation spectrometer.

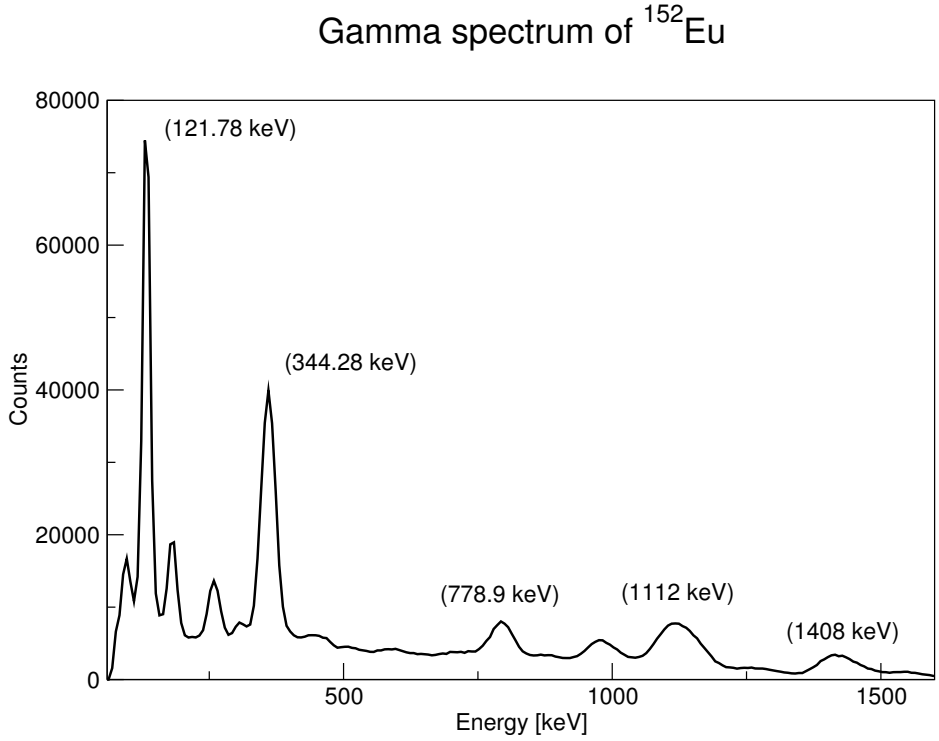

Appendix B

$$^{2}\mathrm{D} + ^{3}\mathrm{T} \rightarrow ^{4}\mathrm{He} + n + Q\ (17.6\ \mathrm{MeV})$$

$$Q + T_d = T_{n'} + T_{\alpha'} \rightarrow \ T_{\alpha'} = Q + T_d - T_{n'}$$

$$p_{\alpha'}^2 = p_d^2 + p_{n'}^2 - 2\ p_d\ p_{n'}\ cos\ \vartheta$$

$$m_\alpha(Q + T_d - T_{n'}) = m_d T_d + m_n T_{n'} - 2\ \sqrt{m_d m_n T_d T_{n'}}\ cos\ \vartheta$$

$$(m_n + m_\alpha)\ T_{n'} - 2\ \sqrt{m_d m_n T_d T_{n'}}\ cos\ \vartheta + T_d\ (m_d - m_\alpha) - m_\alpha\ Q = 0$$

$$T_{n'} = \left(\frac{\sqrt{\frac{m_n \cdot m_d}{m_\alpha^2} \cdot T_d} \cdot cos\ \vartheta + \sqrt{\frac{m_n \cdot m_d}{m_\alpha^2} \cdot T_d \cdot cos^2\vartheta + \left(1 + \frac{m_n}{m_\alpha}\right) \cdot \left(\left(1 - \frac{m_d}{m_\alpha}\right) \cdot T_d + Q\right)}}{1 + \frac{m_n}{m_\alpha}} \right)^2$$

Appendix C

Kinetic energy of neutrons for T(d,n)^{4}He reaction in MeV calculated for various accelaration voltages of deuterium ions (40, 50, 60, 70, 80 keV) with respect to the angle in degrees.

Theta(deg)	40 keV	50 keV	60 keV	70 keV	80 keV
0	14.49721449	14.55325176	14.60447242	14.79763425	14.69673131
10	14.49053466	14.54575609	14.59623402	14.78644771	14.68716198
20	14.47071614	14.52351939	14.57179628	14.75326869	14.65878110
30	14.43841287	14.48728219	14.53197975	14.69922232	14.61255544
40	14.39468554	14.43824469	14.47811344	14.62612956	14.55004903
50	14.34095952	14.37801803	14.4119797	14.53642964	14.47335583
60	14.27896975	14.30856043	14.33574204	14.43307900	14.38501199
70	14.21069544	14.23210201	14.25186059	14.31943313	14.28789348
80	14.13828837	14.15106248	14.16299985	14.19911854	14.18510549
90	14.06399825	14.06796608	14.07193391	14.07590175	14.07986958
100	13.99009848	13.98535763	13.98145352	13.95356199	13.97541439
110	13.91881541	13.9057231	13.89427878	13.83577271	13.87487440
120	13.85226316	13.83141725	13.81298042	13.72599584	13.78120002
130	13.79238581	13.76460019	13.73991140	13.62739122	13.69708102
140	13.74090779	13.70718352	13.67714964	13.54274192	13.62488381
150	13.69929288	13.66078655	13.62645197	13.47439519	13.56660225
160	13.66871168	13.62670193	13.58921854	13.42421782	13.52382071
170	13.65001715	13.60587022	13.56646679	13.39356410	13.49768782
180	13.64372769	13.59886250	13.55881393	13.38325459	13.48889922

Appendix D

Cross section data for ^{63}Cu(n,2n)^{62}Cu reaction for neutrons from 13 MeV to 15 MeV obtained from EXFOR database [20] .

W. Mannhart (2007)

Energy (MeV)	Sigma (mb)	Err (mb)
14.327	512.5	21.78
13.984	433.3	17.42
13.699	411.5	15.72
13.531	383.7	14.24
13.177	301.3	11.15
12.967	255.2	9.09

H. Sakane (2001)

Energy (MeV)	Sigma (mb)	Err (mb)
14.87	538	20.44
14.58	519	17.65
14.28	492	17.71
13.88	441	14.99
13.65	371	12.61
13.40	341	11.94

Y. Ikeda (1994)

Energy (MeV)	Sigma (mb)	Err (mb)
13.3	320	20.00
13.6	360	10.00
13.8	380	10.00
14.0	420	10.00
14.2	450	20.00
14.5	470	10.00
14.7	490	20.00
14.9	510	10.00